Atomistic Simulation of Deformation Induced Rotation in Cu-Nb Composites

by

Ian Chesser

Submitted to the
Department of Materials Science and Engineering
in Partial Fulfillment of the Requirements for the Degree of

Bachelor of Science

at the

Massachusetts Institute of Technology

June 2016

© 2016 Ian Chesser
All rights reserved

The author hereby grants to MIT permission to reproduce and to
distribute publicly paper and electronic copies of this thesis document in whole or in part
in any medium now known or hereafter created.

Signature of Author.....
Department of Materials Science and Engineering
May 2, 2016

Certified by .....
Michael Demkowicz
Associate Professor of Materials Science
Thesis Supervisor

Accepted by .....
Geoffrey Beach
Class of '58 Associate Professor of Materials Science and Engineering
Chairman, Undergraduate Thesis Committee

Atomistic Simulation of Deformation Induced Rotation in Cu-Nb Composites

by

Ian Chesser

Submitted to the Department of Materials Science and Engineering
on May 2, 2016 in Partial Fulfillment of the Requirements for the
Degree of Bachelor of Science

ABSTRACT

Accumulative roll bonding (ARB) of three copper-niobium (Cu-Nb) nano-composite models is simulated using molecular statics techniques to assess the rotational stability of Cu-Nb interfaces at high strains up to 90% thickness reduction. Crystals strain and rotate under compression, and certain Cu-Nb composites have been shown to reach a steady state of rotation at large rolling reductions. These steady-state rotations correspond to the formation of a preferred interface character between layers. Cumulative rotation of Cu and Nb layers was tracked as a function of strain using a rotation algorithm. A Cu-Nb bi-crystal and poly-crystalline model with a {111}<110> Cu || {110}<111> Nb interface character were found to rotate significantly from their initial crystallographic orientation under compression. A Cu-Nb bi-crystal model with a {112}<111>Cu || {112}<110>Nb interface character was found to rotate less when rolled in the transverse direction compared to the typical <111>Cu||<110>Nb rolling direction. Results show that experimentally observed plastic stability of rolled Cu-Nb composites comes from a factor not accounted for in the simulation, like thermally activated dislocation mechanisms. The study refines the current knowledge of plastic stability in Cu-Nb composites.

Thesis Supervisor: Michael Demkowicz
Title: Associate Professor of Materials Science

Acknowledgements

I would like to thank Michael Demkowicz for giving me great advice and keeping me on a clear trajectory throughout the project, and for inspiring curiosity in a topic that initially seemed quite dense. After building atomic models, writing simulations, and analyzing data in new and interesting ways, I have become intrigued by the complex geometries and transformations that occur in microstructures, and will be pursuing a PhD at CMU to study the microstructural evolution of metals.

I would also like to thank Niaz Abdolrahim, now an associate professor at University of Rochester, for getting me up and running with LAMMPS and atomistic simulations. I found the activation barrier for writing MD simulations to be high, and am grateful for her help in getting over this barrier.

A big thanks goes to Diana Farkas from Virginia Tech/NSF for creating the polycrystalline structures copper and niobium structures used in this paper.

Running simulations would not have been possible without Sanket Navale or Dina Yuryev, who set me up on the server and helped me overcome several coding issues.

I am also grateful to Mike Tarkanian and Jeff Grossman for teaching me about materials science in more way than one. Mike got me involved in a metallurgy project in 3.042 that opened my eyes to a fascinating field and became one of my best experiences in Course III. Jeff was an inspiring teacher and team leader for 3.091, and I learned a great amount by TA'ing for his class.

Table of Contents

1. Introduction

1.1. The Need For Better Alloys in Extreme Environments

Current alloys perform poorly in extreme environments that combine high temperatures and stresses with high doses of radiation. The alloys in a nuclear reactor limit the efficiency of the core and the lifetime of the plant as a whole [1]. Zircaloy, a zirconium alloy used as nuclear fuel cladding since the 1950s, is a prime example of an alloy that limits the efficiency and longevity of a nuclear plant. Although zircaloy has a low neutron cross-section, allowing neutrons to pass freely between fuel rods to sustain a nuclear chain reaction, it is limited by radiation-induced embrittlement over time and high temperature oxidation [5-7]. The alloy was implicated in the Fukushima disaster as a source of failure, contributing to overheating of reactor cores through an exothermic oxidation reaction with water [8]. Bulk nano-composites, a new class of advanced alloys, promise increased temperature, stress, and radiation tolerance over Zircaloy. Bulk nano-composites could lead to longer plant lifetimes, less frequent waste disposal, and more reliable waste containment, making nuclear power a viable low emission energy source for the future. Bulk nano-composites also promise better materials for spacecraft, enabling the prolonged exploration of hostile space environments with high temperatures and levels of radiation.

1.2. Putting the "Bulk" in Bulk Nano-materials: Cu-Nb Composites Produced by Accumulative Roll Bonding

Bulk nano-composites derive their bulk properties from the interfaces between alternating, nano-meter size metallic layers. The current problem with bulk nano-composites is one of scale and production. A number of layered nano-composite materials have been made with desirable temperature, radiation, and stress tolerances, but they are limited to lab-scale technologies and cannot be made in large enough quantities for large-scale applications [3]. One truly bulk nano-composite has been made by Mara et al. that successfully encapsulates a desirable set of properties on the scale of a 1m x 0.1 m x 0.2 cm slab [3]. The material consists of alternating layers of copper (Cu) and niobium (Nb) compressed from millimeter layer thickness to nanometer thickness using accumulative roll bonding (ARB) [4]. ARB composites do not develop voids under light-ion irradiation, maintain their structure at temperatures up to half the melting point of Cu, and can sustain stresses exceeding an order of magnitude larger than the strength of either Cu or Nb alone during deformation to large strains >25% [9].

During ARB, a layer of Cu and Nb are joined and compressed via rolling, then cut, stacked, and joined and rolled again as shown in Figure 1. When the layer thickness of Cu and Nb decreases below 800 nm, the distribution of crystallographic orientations in the structure, or texture, is observed to sharpen, corresponding to the development of a preferred interface character free from extrinsic dislocations introduced by plastic deformation [9]. For most polycrystalline bi-metal composites and pure metals, rolling leads to a wide dispersion of crystallographic orientations because of the large number of

misoriented grains that sample orientation space. Each Cu and Nb layer in the final stages of ARB spans only one or two grains, leading to a suppression of certain orientations. ARB produced Cu-Nb is intriguing from a scientific and technological standpoint because it couples deformation and interface evolution in a non-conventional manner to give unprecedented stability against high radiation levels, temperatures, and stresses.

Fundamental understanding linking ARB produced Cu-Nb layers to the production of other bulk nano-materials is missing. This thesis works toward filling this gap with a series of simulated experiments that leverage ARB to try to create a different type of Cu-Nb bulk nano-material.

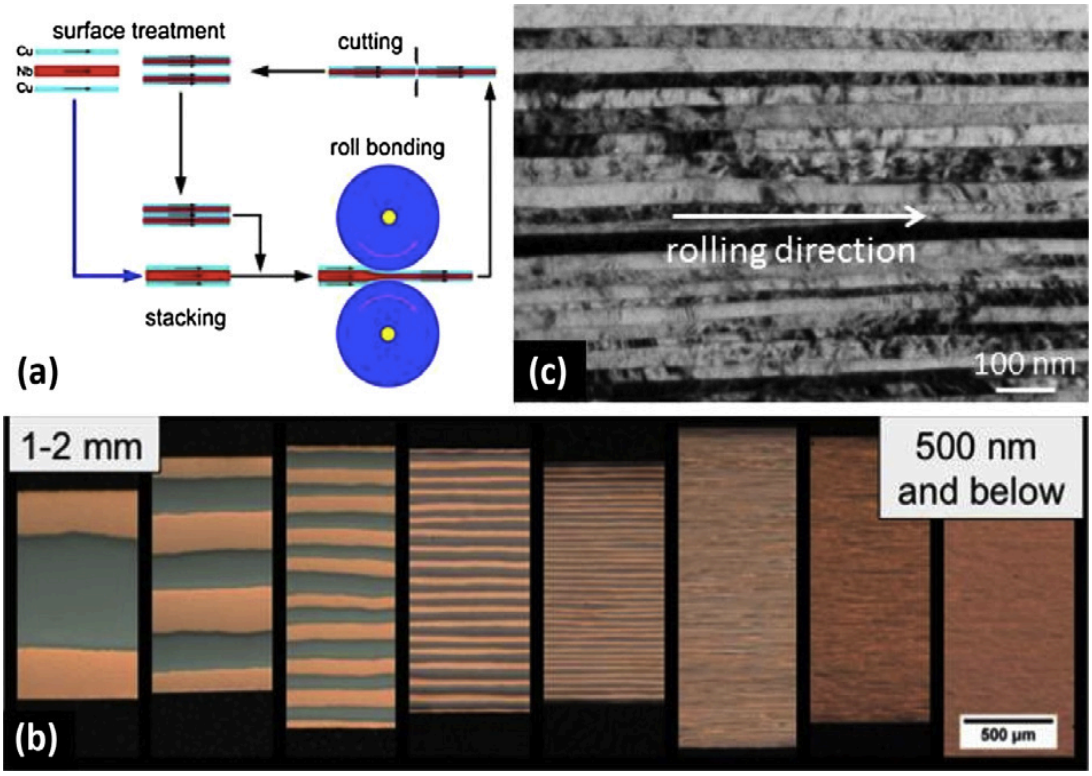

Figure 1: The accumulative roll bonding process consists of repeated stacking, rolling, and cutting steps shown in (a). A sequence of materials cross sections are shown in (b) for Cu-Nb composites with individual layer thickness decreasing from the mm to nm regime. (c) Shows transmission electron microscopy (TEM) micrographs of Cu and Nb layers after rolling reduction to 100 nm thickness. The layers remain remarkably flat. Image taken from [2]

1.3. Leveraging ARB to Scale Up Other Nano-Composites

A sensible choice for a first limited nano-material to try to scale up is physical vapor deposited (PVD) Cu-Nb. In physical vapor deposition, layers of Cu and Nb are sputtered onto a substrate one at a time. PVD produced Cu-Nb composites have a desirable set of radiation, temperature, and stress tolerances, similar to ARB produced Cu-Nb, but have thus far been limited to the micron scale [10]. The interfaces in PVD and ARB produced

Cu-Nb have important similarities and differences. Cu-Nb interfaces in PVD multi-layers differ from ARB interfaces in the crystallographic planes that join at the interface, but both interfaces are free from rolling induced defects and confer a desirable set of properties to the material as a whole. The relevant challenge is leveraging the ARB technique to express other interfaces like the PVD interface in a bulk nano-material.

Consider the following modification to the ARB process for Cu and Nb:
1. Before poly-crystalline Cu and Nb are joined by rolling, a bi-layer of PVD Cu-Nb is deposited between the poly-crystalline layers. We will call this PVD layer the seed layer.
2. The ARB process proceeds as usual, with four new layers added on each stacking step instead of two.

It is possible to simulate such a modified ARB process, which we will call "seeded ARB," with molecular statics techniques. A primary goal of this thesis is to perform a seeded ARB simulation to investigate if seeding of specific interfaces in ARB feedstock can alter the steady state microstructure of a composite under compression. Performing this simulation is worthwhile because it shows which interfaces are stable during the ARB process. Stability is defined as the persistence of a given interface character under deformation. If the PVD interface remains stable at high compressive strains during the ARB process, that would imply that ARB as a technique could be used to scale up previously limited nano-composites like PVD nano-composites. A customized processing pathway for expressing arbitrary interfaces on a bulk scale would be a powerful tool for structural material design, and a seeded ARB simulation is a step toward designing new bulk nano-materials. This work stands to improve our understanding of the ARB process and the viability of nano-composites as structural materials

2. Experimental Models

All experiments proceeded in three steps outlined in Fig. 3 below:
1. Building atomic models as input for an ARB compression simulation
2. Running ARB compression simulation on models up to high plastic strains
3. Analyzing rotations and deformations within the compressed materials

Figure 2: Three stages of experimentation. Building a model, compressing it, and analyzing compressed structure

Each step will be described in detail in the three sections below along with descriptions of relevant models and theory. Three main interface models are simulated: a PVD bi-crystal model, an ARB bi-crystal model, and a poly-crystalline PVD seed model. Cu and Nb layers rotate when a Cu-Nb composite is deformed. The overarching idea of the simulation is to compare the rotation of Cu and Nb layers in the PVD and ARB bi-crystal models to the rotation of Cu and Nb layers in the PVD seed model. If the PVD

interface character is preserved in the PVD seed model under ARB compression, that would imply that ARB as a technique could be leveraged to scale up the interfaces in limited PVD nano-composites to much larger length scales.

2.1. Atomic Models

Atomic models for Cu-Nb nano-composites must approximate the correct interface character between alternating Cu and Nb crystals. An interface has five macroscopic degrees of freedom: two to specify the interface planes $\{h\ k\ l\}$ being joined, and three for the orientation relationship between adjoining crystals [11]. See [38] for a primer on crystallographic notation. The orientation relationship consists of two crystallographic directions $<a\ b\ c>$ constrained to be parallel along the rolling axis and a rotation θ_{twist} of the planes about the interface normal [12]. The interface character of a Cu-Nb interface is summarized in Figure 3. The FCC Cu layer and BCC Nb layer are defined by their respective interface plane and rolling direction $\{h\ k\ l\}<a\ b\ c>$, where RD denotes the rolling direction, ND the normal direction, and TD the transverse direction.

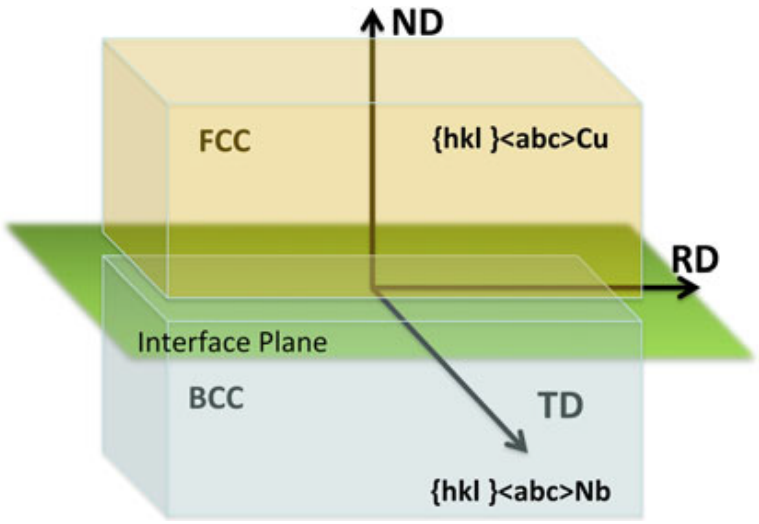

Figure 3: Bi-crystal model with interface character shown as {h k l}<a b c>, where {h k l} is the family of interface planes being joined and <a b c> are the family of directions being joined along the rolling direction (RD). TD denotes transverse direction, ND normal direction. Taken from [20].

PVD and ARB interfaces are experimentally observed to have the following predominant interface characters:

PVD: {111}<110>Cu ‖ {110}<111>Nb
ARB: {112}<111>Cu ‖ {112}<110>Nb (1)

Note that $0° \leq \theta_{twist} \leq 15°$, but is taken to be zero in the simulations described. The orientation relationship for both the PVD and ARB interface is known as the Kurdjumov-Sachs (KS) relation, with a <111> and <110> direction parallel to the rolling direction. Other interface characters are observed in rolled PVD and ARB nano-composites, but

occur less frequently than the characters listed above, and will be ignored in the models that follow.

Both the PVD and ARB interfaces are incoherent, meaning that the mismatch between lattices at the interface is large (> 5%). A periodic array of misfit dislocations form along the interface to relieve coherency strains [4]. Arrays of misfit dislocation act as a supply of dislocations during deformation, and will be discussed further in the results and analysis section. The PVD interface is flat, while the ARB interface is faceted, originating from the different topology of the planes being joined [13].

In addition to the five macroscopic degrees of freedom comprising an interface character, each interface has microscopic degrees of freedom related to the translation of Cu and Nb atoms at the interface. In a molecular statics simulation, a minimization algorithm is applied to an initial structure to adjust the positions of atoms at the interface in a way that minimizes the free energy of the system [12]. Further details about minimization are withheld until section 2.2.

2.1.1. The PVD Model

A PVD model was created with the {111}<110>Cu ‖ {110}<111>Nb interface character in Matlab with $\theta_{twist} = 0°$. A crystal structure is composed of a basis repeated periodically on a lattice. The bases for Cu and Nb layers of the PVD interface are shown below in Figures 4 along with relevant crystallographic directions. The bases are fundamental units used to tile space in three dimensions, and were repeated to construct the slabs of Cu and Nb shown in Figure 5.

The Cu lattice contains 55,176 atoms at a total layer thickness of 7 nm while the Nb lattice contains 36,720 atoms at a total layer thickness of 7 nm. The lattices were joined with an interface spacing equal to the average of the lattice spacing of Cu and Nb in the <111> and <110> directions. Using the equation for distance between crystallographic planes d_{hkl} in terms of a lattice parameter a, taking $a_{Nb} = 3.300$ nm and a_{Cu} = 3.615 nm, we arrive at the desired interface spacing:

$$d_{hkl} = \frac{a}{\sqrt{h^2 + k^2 + l^2}}$$

$$\textit{interface spacing} = \left(\frac{a_{Nb}}{\sqrt{2}} + \frac{a_{Cu}}{\sqrt{3}}\right)/2 \; = \; 2.21 \text{ Å} \qquad (2)$$

The interface between Cu and Nb layers was compared to a reference PVD interface made by *Demkowicz et al* [14]. Both the reference model and the constructed model are used in this paper, with the reference used for stand-alone PVD simulations and the constructed model used for the seeded PVD simulations. The reference interface and constructed interface are compared in Figure 6. The two interface planes are mirror images of each other with equivalent interface character. Differences in the models will be discussed in the context of the PVD seed model in the next section. The atomic models in Figures 5-6 are visualized in Ovito, an atomic visualization software [15]. The models are colored according to adaptive common neighbor analysis (CNA), with perfect FCC atoms with twelve nearest neighbors colored green and perfect BCC atoms with eight nearest neighbors colored blue [16].

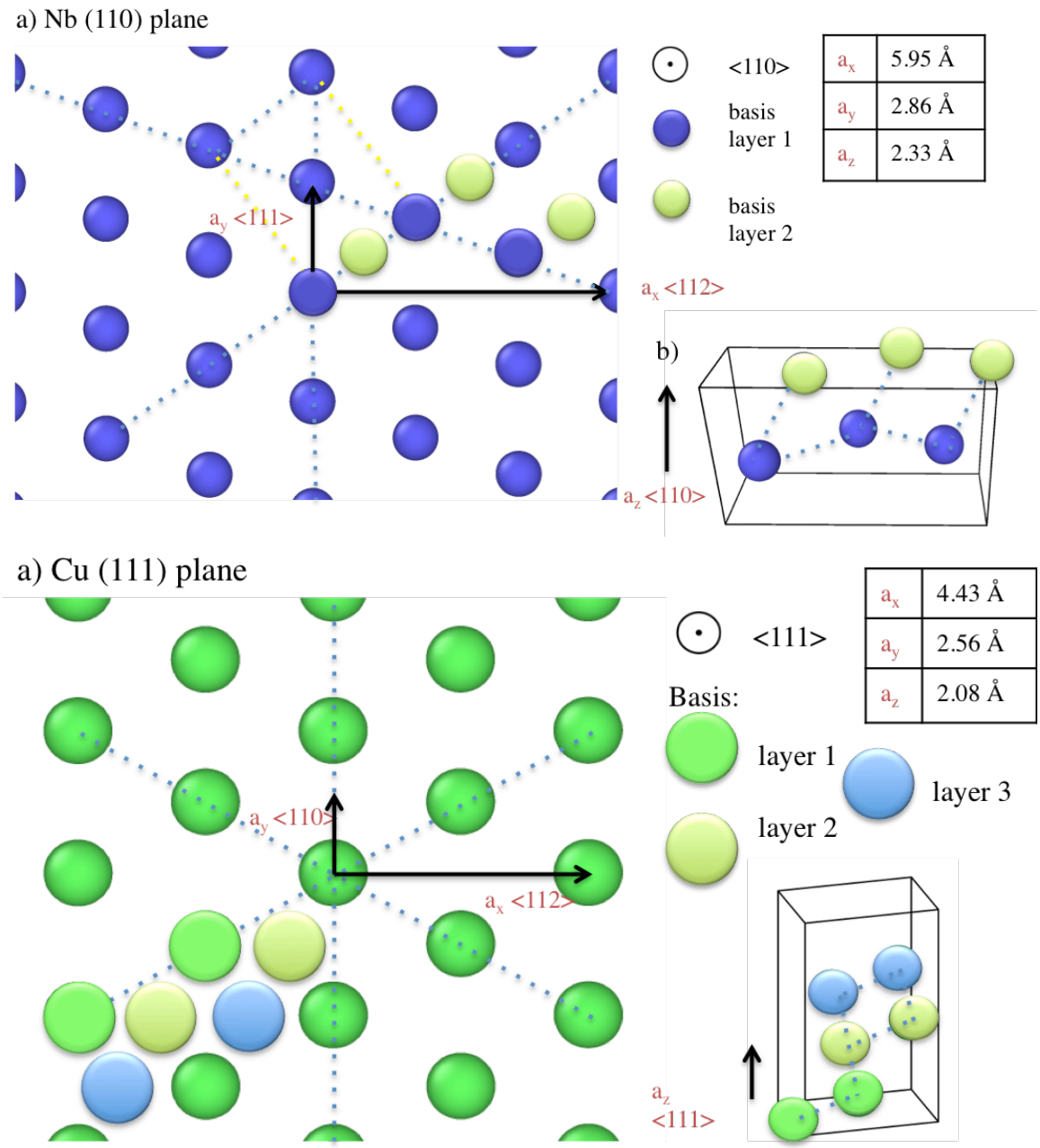

Figure 4: Nb (110) in blue (a) and Cu (111) plane in green (b) with out of plane basis atoms colored to illustrate stacking pattern of lattice. Six atom basis for Nb and Cu shown in the bottom right hand side of each diagram.

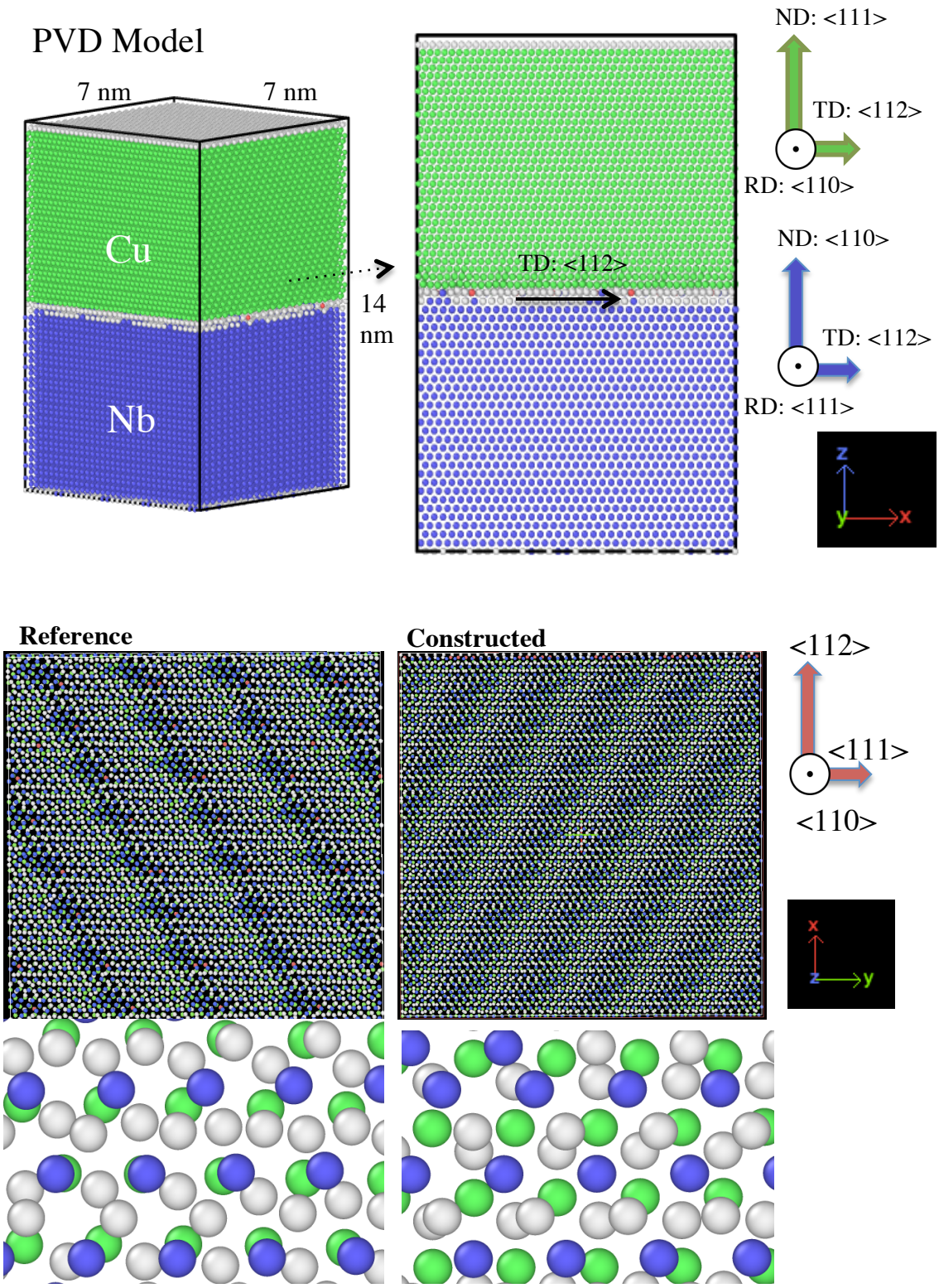

Figure 5,6: Fig. 5 shows front view of PVD model, where Cu and Nb are joined in the TD along <112> planes. Figure 5 shows a comparison of the reference interface and constructed interface zoomed out on top (10 nm x 10 nm) and zoomed in on bottom (10 Å x 8 Å). The interfaces are mirror images.

2.1.2. PVD seed model

Polycrystalline metals containing grains of varying size and orientation. Neighboring grains share a grain boundary across which crystallographic orientation changes discontinuously [17]. During ARB, Cu and Nb layers are refined to the thickness of one or two grains and a stable interface character develops. To simulate the seeded ARB process, polycrystalline slabs of Cu and Nb are made to encapsulate a PVD bi-crystal seed, as shown in Figure 8. The poly-crystalline slabs were constructed by Diana Farkas at Virginia Tech using a Voronoi algorithm [18]. Each slab used spans two grains in every direction with an average grain diameter of roughly 100 nm. The model contains 265,200 Cu atoms and 170,988 Nb atoms with a total Cu thickness of 22 nm and a total Nb thickness of 22 nm. The PVD seed layer contributes 8 nm of thickness to the Cu layer and 8 nm to the Nb layer. The entire model has initial x/y/z dimensions of 12.0 nm, 11.9 nm, and 44.2 nm.

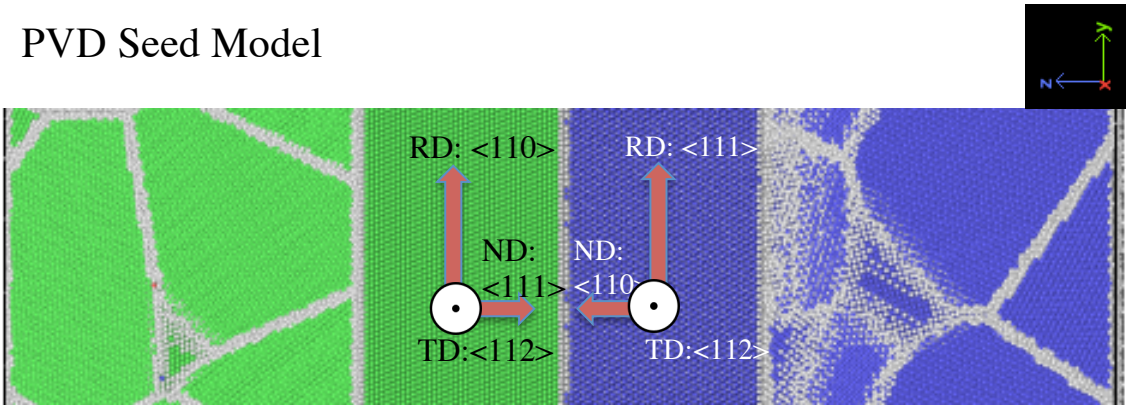

Figure 7: Side view of PVD seed model shown with interface planes joined along the rolling direction. Model rotated to save space, with simulation box axes shown in the upper right corner. From left to right: poly-Cu, PVD Cu, PVD Nb, poly-Nb. See scale in description above.

One feature of all the atomic models discussed in this paper is that they must satisfy periodic boundary conditions in three dimensions. Periodic boundary conditions are a trick to approximate a large system with a finite volume of material. When an atom gets squeezed out of one side of the simulation box during compression, it enters through the adjacent side. By the minimum image convention, atoms on faces, edges, and corners of an orthorhombic simulation box interact with atoms on opposite faces, edges, and corners. In this way, a small system is tricked into behaving like an infinite system. For the initial PVD seed model, periodic boundary conditions must be satisfied in both the poly-crystals and the seed layer.

In this experiment, the dimensions of the constructed PVD seed model had to be matched to the dimensions of the poly-crystals as given in the x and y directions to satisfy periodic boundary conditions. The dimensions of the seed model can only be modified by integer multiples of the basis lengths, and an issue arose when no integer multiple of the basis lengths for Cu and Nb closely matched the x and y width of the Cu and Nb

poly-crystals. To overcome the mismatch problem, a volume conserving strain was imposed on the constructed Cu and Nb crystals to match the x and y width of the poly-crystals:

$$\varepsilon_{x,Nb} = -0.009,\ \varepsilon_{y,Nb} = 0.0091,\ \varepsilon_{x,Cu} = 0.0034,\ \varepsilon_{y,Cu} = -0.0033 \quad (3)$$

A volume conserving strain matches the volume conserving assumption of the ARB compression simulation, discussed in section 2.2. A final detail about the seed model involves the spacing between the single crystal and poly-crystalline Cu layers and the single crystal and poly-crystalline Nb layers. Pressures in the simulation are sensitive to initial simulation box sizes. Spacings between layers contribute to the length of the simulation box in the z direction, and must be within a certain range to avoid large initial pressures on the minimized structure. Starting with a spacing of $d_{111,Cu} = 2.09\ nm$ between Cu and poly-Cu and a spacing of $d_{110,Nb} = 2.33\ nm$ between Nb and poly-Nb, spacings were iteratively modified to minimize pressure in the z direction, with a final initial spacing of $1.60\ nm$ for Cu and $1.90\ nm$ for Nb. These values stand to be further optimized.

Pre-straining a model will generally lead to different values for quantities like interface energy in a minimized structure. The reference PVD model, for instance, has a plane strain applied to a monolayer of Cu above the Cu-Nb interface to improve coordination between Cu and Nb at the interface. Such straining leads to an energetically favorable interface structure after minimization despite an elastic energy penalty because of an increase of coordination of Cu and Nb atoms at the interface [19].

The compression simulations involve strains of up to 90% thickness reduction in the z-direction. Since the focus of the study is on large plastic strain behavior of Cu-Nb models, initial differences in strain state between the reference PVD model and PVD seed model are assumed to be negligible.

2.1.3. ARB Model

A bi-crystal with a {112}<111>Cu ‖ {112}<110>Nb ARB interface character is another atomic model considered as a benchmark for the results of the PVD seed model. The model originates from the work of *Demkowicz et al*., with several differences [11]. The model has been rotated so that the interface normal aligns with the z-axis of the simulation box and has been modified to enforce periodic boundary conditions in the z-direction. The interface spacing between the top and bottom of the model was iteratively adjusted to minimize pressures in the system.

A perspective view of the ARB model is shown in Fig. 9. The xz plane shows aligned <110> and <111> planes of Cu and Nb. The yz plane shows the faceted structure of the {112} planes joined at the interface, with facets along <111> and <110> directions. A network of partial dislocations is identified in red by CNA in Ovito. A partial dislocation has a Burgers vector that is not a translational vector of the Cu lattice. The red coloring corresponds to the hexagonal close packed arrangement of atoms around the partial dislocations. The ARB interface accommodates two other distinct sets of dislocations in addition to the partial dislocations [20].

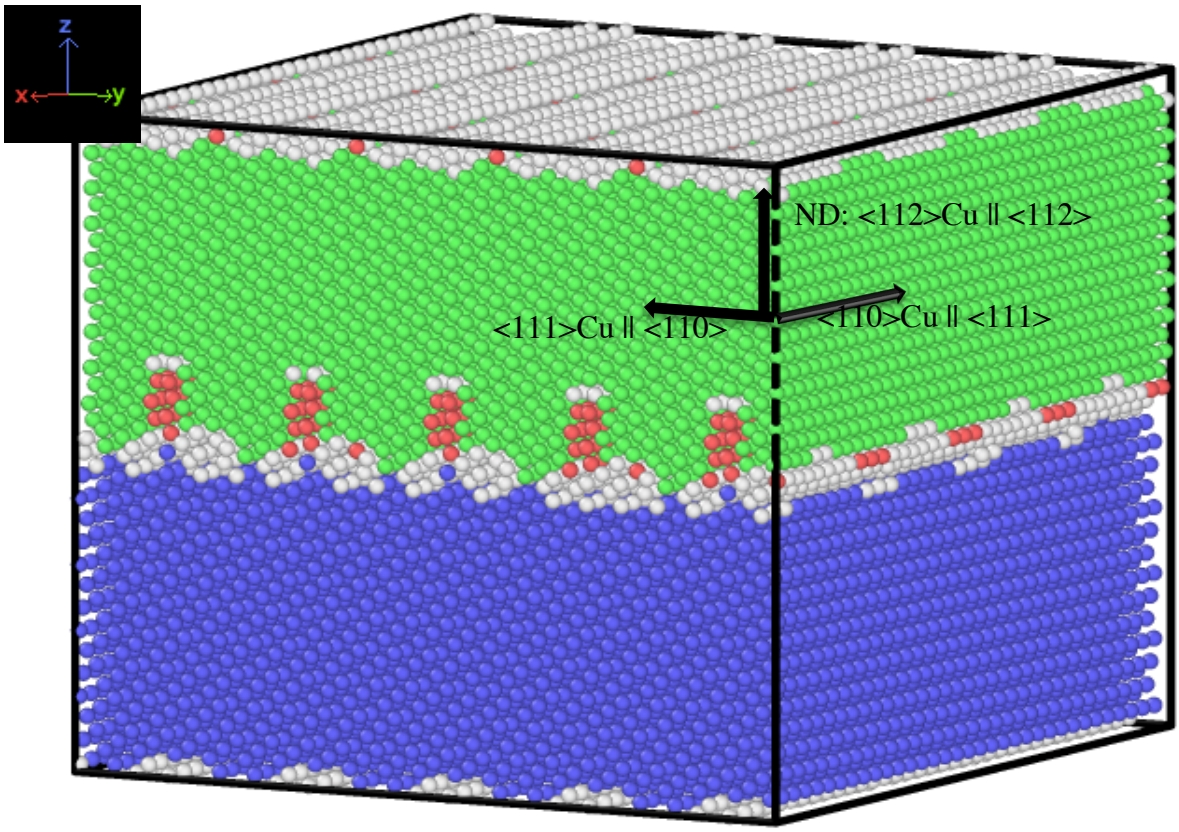

Figure 8: Perspective view of ARB interface model. Faceted yz plane develops in response to a <111> Cu direction being joined to a <110> Nb direction.

2.1.4. Other Models

Other models considered include single crystals of Cu and Nb with (111) and (110) planes normal to the compression axis, Cu and Nb poly-crystals, and a polycrystalline Cu-Nb model without a PVD seed layer. A previously uncharacterized Cu-Nb model with a {111}<110>Cu ‖ {110}<110>Nb interface character was also constructed. We denote the orientation relationship of this interface the Chesser-Demkowicz orientation relation (CD). The CD model was seeded between polycrystalline Cu and Nb, and compression of the seeded CD structure could offer further insight into how Cu-Nb interfaces evolve at extreme strains.

2.2. Compression Simulation

Atomic structures are compressed to 10% of their original thickness in the interface normal direction using molecular statics techniques, corresponding to a 90% reduction in individual layer thickness. The interface normal direction corresponds to the z-axis in all simulations. Experimental rolling studies have only gone to 50% thickness reduction for PVD interfaces [21, 22].

Compression simulations were written in LAMMPS, a molecular dynamics software, and run on a remote server [23]. Steps in the simulation are listed below:

1. Read in Cu-Nb structure with periodic boundary conditions
2. Associate structure with EAM potential
3. Minimize structure with pressures in x,y,z fixed to zero
4. Compress simulation box in z by small increment, expanding along RD to conserve volume
5. Minimize compressed structure, output data
6. Repeat 4 and 5 until 90% thickness reduction in z

After being read into LAMMPS with periodic boundary conditions, the atomic model is associated with a many-body potential that represents interatomic forces between atoms in the Cu-Nb model. The accuracy of many-body potentials is crucial to obtaining atomistic results that approximate reality. The Cu-Nb simulations use a potential constructed via the embedded atom method (EAM) by Mishin *et al*. [24]. Many alloys beyond one and two component systems lack empirically accurate potentials.

The Cu-Nb structure is initially minimized using the conjugate gradient algorithm, whereby atoms iteratively move from their initial positions in a direction of energy decrease until the structure reaches a local energy minimum [25]. The minimization is subject to an additional pressure constraint where pressures are driven to zero in the x,y,z direction by iteratively adjusting the size of the simulation box. To approximate a real system, the initial, uncompressed structure should have low pressures in all directions. Because the objective function being minimized changes with box size, minimizing the energy of the system while driving the pressures to zero is an ill-defined problem sensitive to initial simulation box size. The algorithm can get stuck before reaching the desired pressure tolerance. This problem is particularly relevant to the PVD seed model, which contains four lattices of slightly different dimensions. One solution to overcome this problem is to run multiple minimizations in succession. Reaching desired pressure tolerances more accurately is an area of continued work in this project.

After the initial pressure fixing and minimization, the Cu-Nb structure is compressed by deforming the simulation box and minimizing the resultant structure. This two-step process comprises one compression step. Two observations about ARB inform the nature of the applied compression:

1. During ARB, the dimensions of the sheet metal in the rolling direction are observed to increase while the dimensions of the metal in the transverse direction remain approximately fixed because of friction between metal and roller.
2. ARB reaches high plastic strains, and plasticity conserves volume. Therefore ARB compression can be approximated as volume conserving.

A volume conserving strain is imposed on the simulation box, with compression in the z-direction and tension in the rolling direction. The transverse direction in the model is held at constant length. For stand-alone PVD and ARB models, 900 compression steps were performed at strains of $\varepsilon_z = 0.001$ corresponding to 0.1% thickness reduction along the z-axis per step and expansion in the RD by approximately 0.1% per step. Ninety steps at 1% compression along the z-axis were performed for the PVD seed model. Larger step sizes were chosen because of the longer overall runtime of

the simulation. The molecular statics simulation for the PVD seed model takes around a week to reach a hundred compression steps on 128 processors, whereas the stand-alone PVD and ARB simulations take one or two days for 900 steps on 64 processors.

Molecular statics (MS) simulations assume zero temperature, and therefore negate thermally activated dislocation mechanisms. The zero temperature assumption is not assumed in molecular dynamics (MD). In MD simulations, different thermodynamic ensembles are applied to simulate processes at finite temperatures. MS simulations have the advantage of being simpler than MD simulations, and can be augmented with MD simulations at higher temperatures as necessary.

In molecular statics simulations, drops in energy associated with dislocation motion may cause problems for minimization algorithms that require continuous derivatives of energy for calculations. Because of these issues, the level of uncertainty of predicting stress-strain curves by MS techniques for real crystals are high [26]. Predicting accurate moduli values is not the focus of this study, however, and stress-strain data generated by MS techniques provides an internally consistent framework for comparing deformation processes of different models. MS is thus sufficient for comparing the deformation of the stand-alone PVD and ARB interfaces to the deformation of the PVD seed model.

2.3. Rotation Analysis

Before diving into rotation analysis, it is important to understand slip as a deformation mechanism in metals. When a single metal crystal is plastically deformed, discrete steps are observed on the surface of the metal under a microscope. These steps are a result of planes of atoms slipping past each other. Slip corresponds to the passage of many line defects called dislocations through the material. A heavily cold rolled metal has 10^{14}-10^{15} dislocations per square meter, corresponding to roughly one dislocation per 30 – 100 nm [30]. Slip occurs preferentially on closest packed planes in FCC and BCC crystals because those planes have the smallest spacing between atoms and therefore the smallest unit slip distance. A slip system is characterized by a slip direction along a slip plane denoted <dir>{plane}. FCC materials like Cu have 12 independent slip systems of type <110>{111}, while BCC materials like Nb have 12 independent slip systems of type <111>{110}, 24 of type <111>{112}, and 12 of type <111>{123} for a total of 48 possible slip systems. Many analyses focus on identifying which slip systems are active during plastic deformation. The focus of the present analysis is rotation caused by slip. Fig. 10 shows a schematic of a single crystal undergoing slip under a tensile load. To accommodate the continued load and slip, the lattice as a whole rotates, as seen in Figure 9 below. Note that the rectangles highlighted also undergo a strain.

Incremental plastic strain and plastic rotation due to a unit slip step can be expressed as tensors $d\varepsilon_{ij}^{p}$ and $d\omega_{ij}^{p}$, where [30]:

$$d\varepsilon_{ij}^{p} = \alpha_{ij} b \rho dx \quad (4)$$

$$d\omega_{ij}^{p} = \beta_{ij} b \rho dx \quad (5)$$

Ignoring the α_{ij} and β_{ij} pre-factors initially, b is the unit slip distance of the deformation. b is the magnitude of a quantity called the burgers vectors, which describes

the magnitude and direction of lattice distortion resulting from a single dislocation. ρ is the dislocation density, and α_{ij} and β_{ij} are tensor coordinate transformations that resolve strain and rotation in the direction of applied strain. $\hat{b}_i$ represent components of the unit vector in the slip direction and $\hat{n}_i$ the components of the unit normal to the slip plane.

$$\alpha_{ij} = \frac{1}{2}\left(\hat{b}_i\hat{n}_j + \hat{b}_j\hat{n}_i\right) \quad (6)$$

$$\beta_{ij} = \frac{1}{2}\left(\hat{b}_i\hat{n}_j - \hat{b}_j\hat{n}_i\right) \quad (7)$$

The goal of the present rotation analysis is to track the rotation of Cu and Nb layers subjected to large plastic strains. Equations 4-7 are useful validations for strain and rotation data generated, but would be difficult to extract from the raw data outputted by the simulation. The simulation outputs a list of coordinates for each compressed structure along with the simulation box lengths and pressures normal to the box. Continuum mechanics offers a way to analyze the rotations and deformations in a compressed structure.

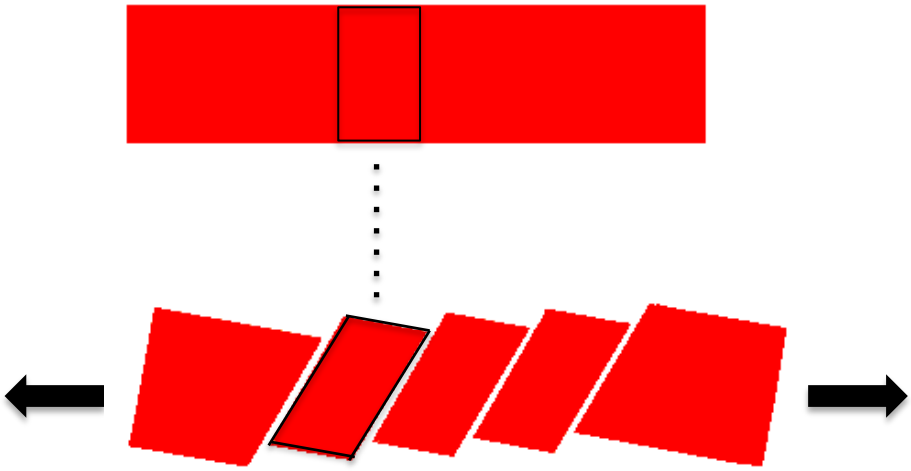

Figure 9: Schematic diagram of slip in a single crystal under tension. The rectangle outlined in black undergoes a strain and a rotation. Figure modified from [39]

Deformation in a material can be defined by a tensor that maps position vectors of atoms in a reference state to position vectors in a current, deformed state. This tensor is known as the deformation gradient, denoted F in equation (4) below:

$$V_{current} = F\,V_{reference} \quad (8)$$

F can be uniquely decomposed into a rotation and stretch R and S, such that

$$F = R\,S \quad (9)$$

R is orthogonal and S is symmetric, meaning that $RR^T = I$ and $S = S^T$, where I is the identity matrix. Using these identities, we find an expression for S and R in terms of F:

$$F^TF = S^TR^TR\,S = S^TS = S^2 \rightarrow S = \sqrt{F^TF},\ R = FS^{-1} \quad (10)$$

S is known as the right Cauchy strain tensor.

$V_{current}$ and $V_{reference}$ can be taken as 3×3 matrices containing three nearest neighbor vectors, one in each row. Let the current configuration be compression step $i+1$ and the reference configuration compression step $i \rightarrow V_{i+1} = F_i\,V_i$. Solving for F_i and then

S_i and R_i via (6), we can track the relative rotations and stretches between compression steps.

Rotation matrices can be converted into different representations of rotations surveyed in [31]. A simple representation is an angle-axis pair $(\hat{n}_i, \theta)$. Any rotation or sequence of rotations in space can be represented by a rotation θ about a single axis $\hat{n}_i$, where $\hat{n}_i$ is a unit vector with three components. Note that $\hat{n}_i$ is different from the same symbol in (6) and (7). All rotation matrices are converted to angle-axis pairs in the rotation results that follow.

Pseudo-code that implements the rotation-tracking algorithm is given below:

```
1  Read in initial uncompressed structure
2  Build nearest neighbor list for structure, choose three nearest neighbor vectors
3  for i = 1 : number of steps
4          Read in structures i and i+1
5          for atom ID in ID list
6                  Find nn vectors on steps i and i+1 using info from nn list
7                  Solve for F_i, R_i, S_i
8                  Extract angle-axis pairs
9                  Store data
10         end
11 end
```

Building a nearest neighbor list entails finding and recording all of the atoms within a certain cut-off distance of the atom being searched, and doing this for all atoms in the initial model. The runtime for the brute-force implementation, which searches the entire model for the nearest neighbors of each atom, scales as $O(n^2)$, where n is the number of atoms in the model. This runtime is prohibitively slow. The built-in Matlab function *rangesearch* is used instead, and implements a k-d tree data structure to find nearest neighbors within a given cut-off radius with a worst-case run-time of $O(n)$ [27]. The cut-off radius was set to the average distance between the first and second nearest neighbors for Cu and Nb, respectively, depending on which material was being analyzed:

$$r_{c,Cu} = 3.087 \text{ Å}, \quad r_{c,Nb} = 3.983 \text{ Å} \tag{11}$$

The nearest neighbor search generates a list of atomic ID's that correspond to the ID's of the nearest neighbors of the atom being searched. The coordinates of the atom being searched are subtracted from the coordinates of the nearest neighbor atoms to generate a list of nearest neighbor vectors. Three vectors are chosen to be non-coplanar and used as a reference for the rest of the simulation. Note that a coplanar set of three vectors can lead to singularities in the deformation gradient.

The rotation algorithm loops over the compressed output structures, calculating the nearest neighbor vectors of subsequent structures and extracting deformation gradients, rotation matrices, and stretch matrices via equation (6). To calculate nearest neighbor vectors, the algorithm only needs to use the ID information generated in the initial nearest neighbor list.

Three caveats must be addressed to extract meaningful rotation data from the simulation. The third caveat is the most important and most difficult to handle:

1. Initial neighbor list building does not take into account periodic boundary conditions. An atom on a face, edge, or corner of the simulation box will not be able to find all of its neighbors. For this reason, only atoms in the interior of a given Cu-Nb model are considered that are not on faces, edges, or corners of the model. This means that a smaller total volume of material is analyzed than the volume of the simulation box. Several options for overcoming this issue include implementing the linked cell algorithm, running the nearest neighbor search on a superstructure periodically wrapped with images of itself, or considering different sets of nearest neighbor vectors locally so that the initial vectors never extend outside the simulation box [28].

2. During the simulation, atoms can move out of the simulation box through one side and in through the opposite side. A distance metric must be used which correctly tracks atoms in a periodically wrapped lattice. A distance function is implemented that obeys the minimum image criterion [29].

3. During deformation, atoms can get caught in the cores of dislocations. Atoms that were initially nearest neighbors can get moved far apart after a dislocation moves through the region, leading to large stretches and widely varying rotations. To avoid looking at atoms caught in dislocation cores, we only consider rotations for atoms with well-behaved stretches. What constitutes a well-behaved stretch will be designated and described in the analysis section.

3. Analysis & Results

The goal of this section is to quantify the amount that Cu and Nb layers rotate in compressed Cu-Nb models and observe the atomistic mechanisms that lead to rotation. Rotations in the ARB and PVD models are compared to the rotation of the PVD seed model. The three main benchmarks for comparison are stress-strain curves, visualized dislocation mechanisms, and rotation plots. The stand-alone PVD model is analyzed first, followed by the ARB model and finally the PVD seed model. In analyzing the PVD model a tutorial approach is taken to help the reader internalize why regions of the Cu and Nb lattices rotate, how the rotation analysis works, and the limitations of the presented analysis.

Experimentally compressed Cu-Nb layers with the PVD and ARB interface character are not observed to deviate significantly from their initial orientations. This means that neither Cu nor Nb rotates significantly about the rolling direction. Since the PVD and ARB composites preserve a stable interface character at high strains, they are considered plastically stable.

In terms of rotation, plastic stability could be borne out in an atomistic simulation in two ways:
1. Small overall rotations at high strains
2. A steady-state rotation converged to at high strains

3.1. PVD Model

3.1.1. Stress Strain Curves For Rolling in Two Directions

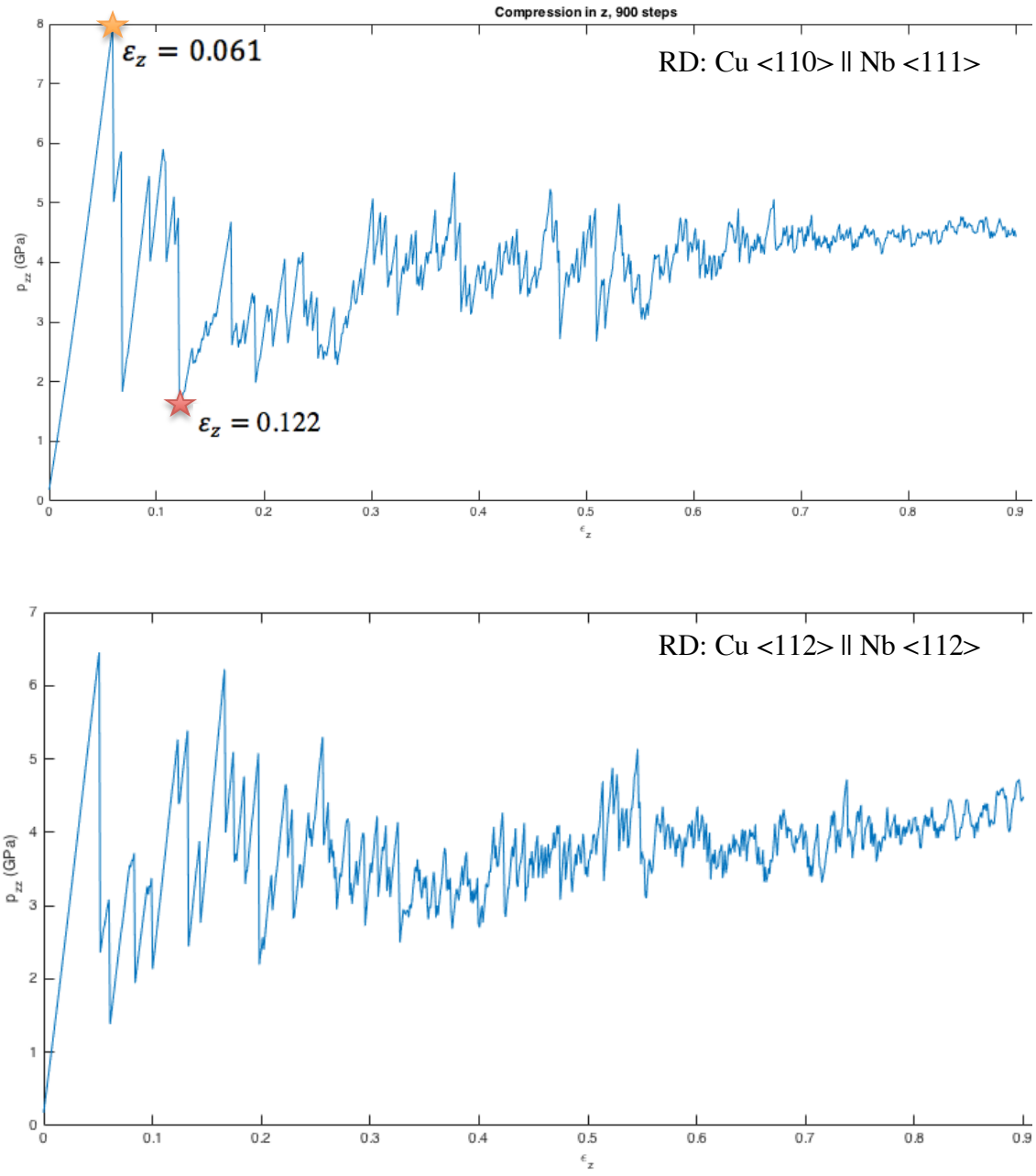

Fig 10 – Stress strain curve for PVD model compressed to strains of 90% in z (ND), expanded along the <110>Cu || <111> Nb rolling direction (top) and <112>Cu || <112> Nb rolling direction (bottom). Orange and red stars correspond to point that will be visualized.

Two different compression simulations were run on the PVD model, one with compression in z and tension in y, the other with compression in z and tension in x. The y-direction corresponds to the <110>Cu || <111> Nb rolling direction and the x direction corresponds to the <112>Cu || <112> Nb transverse direction. The first simulation represents rolling along the typical, experimentally observed texture for PVD interfaces, while the second represents rolling along the transverse direction. The second simulation was run to probe for in plane anisotropies in the deformation response of the PVD composite [31]. The stress-strain curves for compression along the z-axis are shown for both models in Figure 10 on the previous page, and are largely similar, indicating little anisotropy in the stress response to plastic deformation.

The PVD composite rolled in the transverse direction has a slightly lower yield stress and strain than the other PVD composite by 500 MPa and 1% strain. Both materials go through cycles of strain hardening and strain softening and reach an approximate steady state of stress past 60% strain at ~ 4 GPa. High values for yield stresses four times greater than experimentally observed values ~1-2.5 GPa can be rationalized by the fact that the simulation is performed at zero temperature with pure crystals that lack grain boundaries. Tension in the rolling direction, which was analyzed but not plotted, is similar for both models.

3.1.2. Linking Deformation to Dislocation Activity and Rotation

Jumps in stress can be linked to dislocation activity in the bi-crystal and rotations in the Cu and Nb lattices. In this section we will only focus on the rolling simulation along the <110>Cu || <111> Nb direction, since the simulation in the transverse direction is similar. Figure 11 shows a side view of the Cu-Nb model before and after plastic deformation at 5.9% strain and 6.8% strain, with red marker atoms indicated to show rotation of the lattice. A rotation in the Cu layer is observed at the onset of plastic deformation, but not in the Nb layer, indicating that the Cu layer yields first. Cu has lower yield strength than Nb, and previous atomistic simulations have shown that misfit dislocations emit dislocation loops into Cu at the onset of plastic deformation before Nb [13]. Figure 11 shows that at 6.8% strain a network of dislocations has protruded into the Nb layer. At 6.9% strain the Nb layer is observed to rotate, corresponding to the disappearance of the network of dislocations shown in the figure. The rotation of Nb and "collapse" of the dislocation network in Nb indicates that a dislocation loop has moved through the layer.

Deformation of Cu and Nb layers in bi-metallic nano-composites with layer thickness from 5-100 nm has been shown to correspond to confined layer slip [32]. In confined layer slip, the stress field of a dislocation approaching the interface locally shears the interface, resulting in spreading of the dislocation core and dislocation trapping at the interface plane. Cu-Nb nano-composites are weak in shear, the reason that confined layer slip happens in the first place. The interface acts as a warehouse for dislocations that can be distributed along slip planes in either the Cu or Nb layer or both at once.

Figure 12 delves further into the dislocation mechanics of PVD compression. A PVD model is shown at 12.1% strain on the left and 12.2% strain on the right. The model on the right corresponds to the stress minimum marked with a red star in the top of Figure 10, while the model on the left corresponds to the first strain hardening peak to the left of

the star. Three representations of the model in Figure 12 demonstrate atomistic rotation and hardening mechanisms. Moving from the top to bottom of the figure:

Top: Red marker atoms are shown in Cu and Nb layers. Both layers show a rotation. The rotated Cu layer shows mores "steps" in the distorted red region than the rotated Nb layer, indicating that the Cu has rotated more than Nb. In general, every time a dislocation passes through a region, that region should rotate.

Middle/bottom: All perfect FCC Cu and BCC Cu atoms have been removed in the middle representation so that only atoms in dislocations or at the interface are visualized. Atoms marked in light red have hexagonal close packed coordination (HCP). HCP coordination is characteristic of Shockley partials, which are 1/6<112> defects shown as the green line defects in the bottom figure. 1/6<112> means that the dislocation extends 1/6 the length of the lattice parameter for Cu in a <112> direction. Shockley partials can accommodate further stresses by growing into stacking faults, or can stabilize into structures like the tetrahedra shown in the middle and bottom right of Figure 12. These structures are known as stacking fault tetrahedra, and are composed of 1/6<110> dislocations named stair-rod dislocations, shown in purple. Stacking fault tetrahedra are a significant source of strain hardening in FCC materials because they block the motion of other dislocations at the interface [33].

The bottom figure is generated with DXA analysis in Ovito, a program that maps out line defects in FCC materials via conservation of Burgers vectors [34]. Dislocation structures in BCC materials are hard to diagnose because of the large number of possible slip planes. The large number of slip planes explain how the column-like structures in the Nb layer of Figure 12 are formed: a dislocation can glide along a <110> direction and continuously change slip plane, taking a winding path up through a layer in the direction of applied load. Nb column structures such as those in Figure 3 are observed to contribute to strain hardening throughout the simulation in addition to stacking fault tetrahedra in Cu.

At high strains >40% dislocations are observed to transmit across the interface. At 50% strain, the Cu and Nb layer are 3.5 nm in thickness, compressed from an initial thickness of 7 nm. Below ~5 nm layer thickness, bimetallic nano-composites are often observed to deform via slip transfer across the interface plane, a different deformation mechanism than confined layer slip. The observation of interface crossing is thus consistent with the length-scale being observed. Interface crossing accompanies a high density of dislocation in both the Cu and Nb layers, and a high density of stacking faults in the Cu layer shown in Figure 13. It should be noted that the prime focus of this study is not to identify the deformation regimes of Cu-Nb nano-composites, but the rotation of each Cu and Nb layer during deformation. The relevant point is that different regimes of deformation exist based on the dislocation mechanisms at play at different length-scales, all of which can lead rotations in the Cu and Nb lattices.

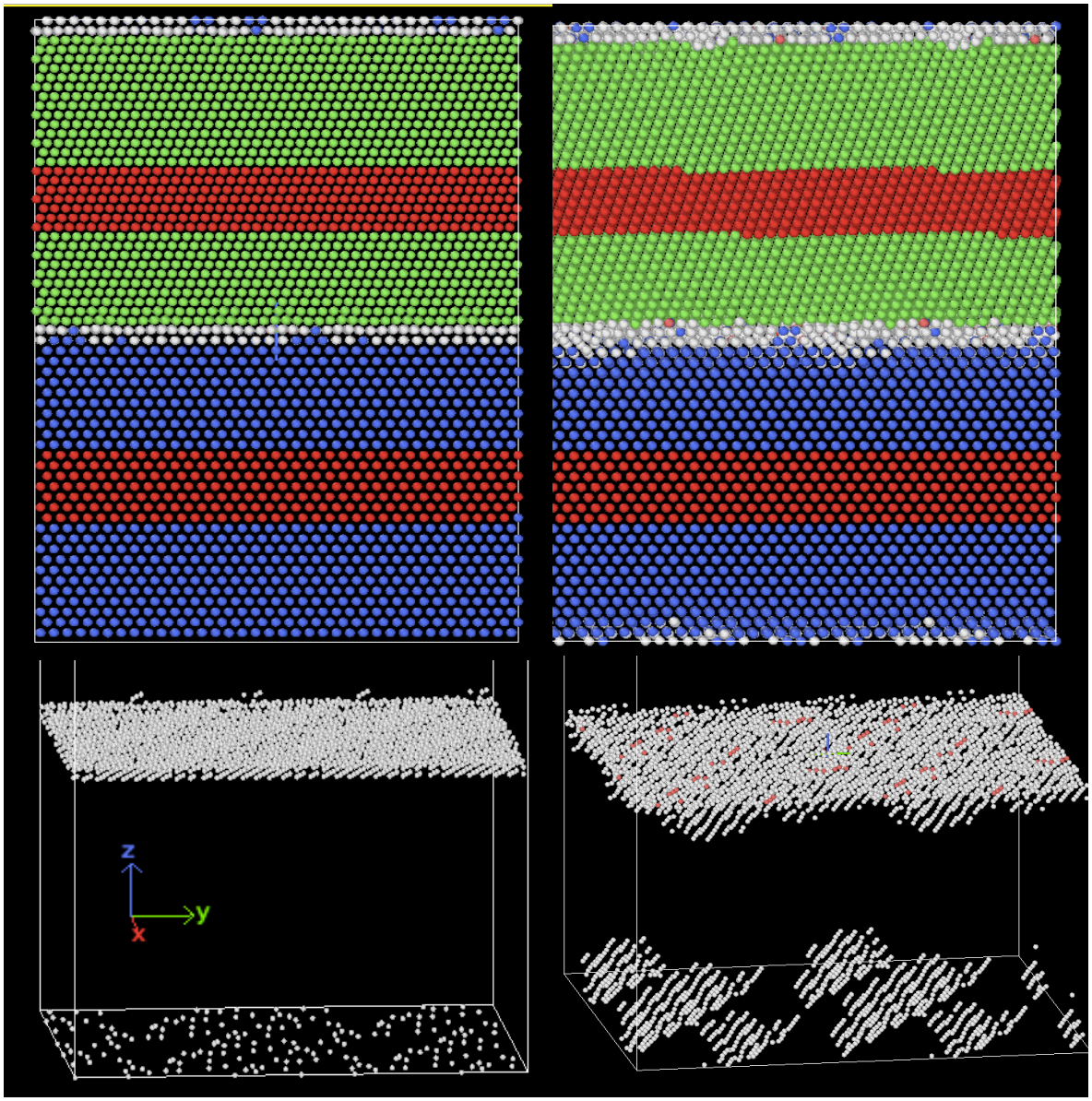

Figure 11 – PVD model before and after plastic deformation at 5.9% strain (left) and 6.8% strain (right). Red marker atoms on Cu and Nb layers show that Cu rotates before Nb, which remains un-rotated. Bottom models show interface before and after plastic deformation.

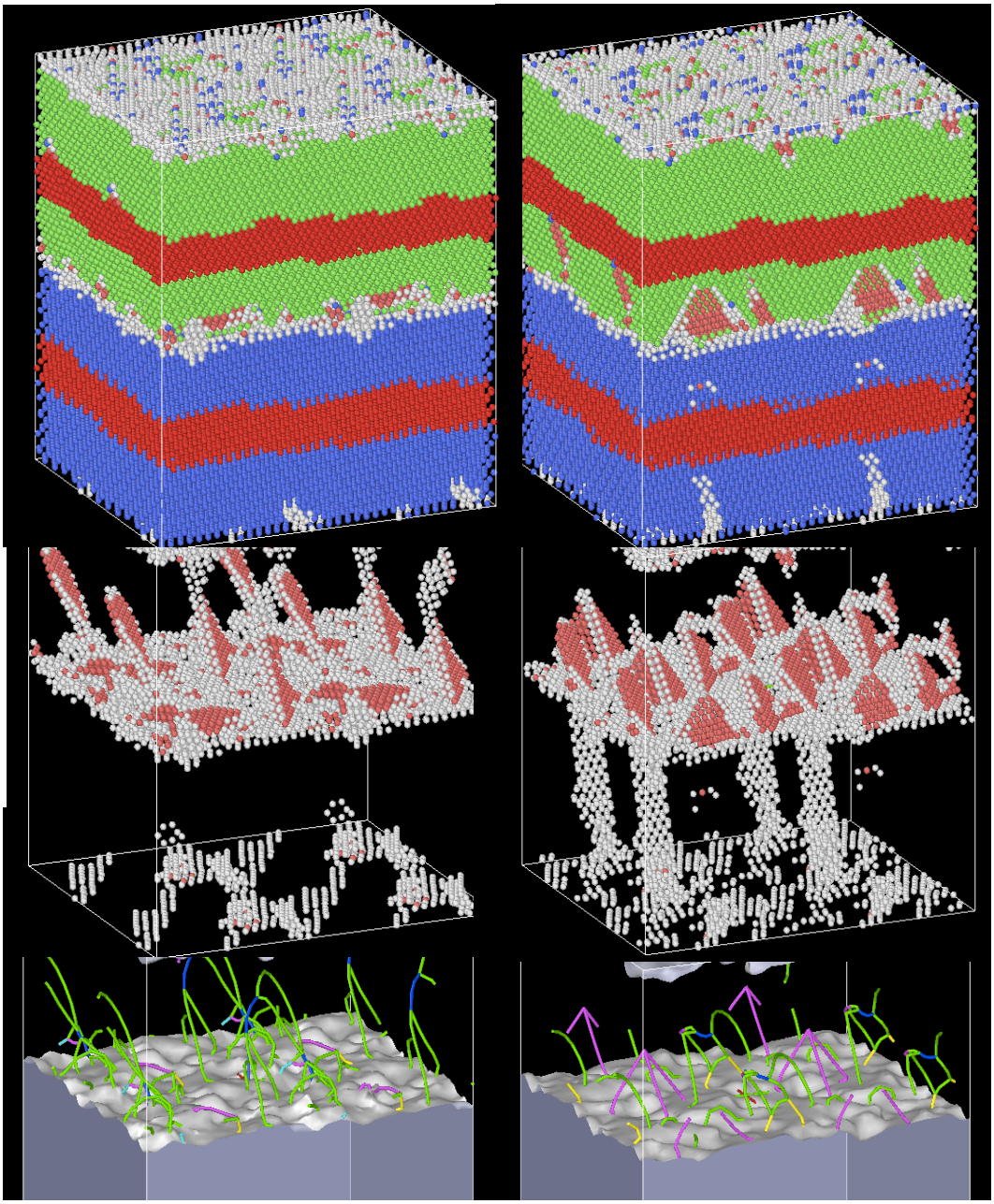

Figure 12 – PVD model at 12.1% strain (left) and 12.2% (right).
Three perspective shown, from top to bottom:
Top: common neighbor analysis with marker atoms to show rotation, **Middle:** common neighbor analysis with all perfect FCC and BCC atoms deleted, showing only HCP atoms in red or atoms that have no distinguished coordination in white. **Bottom**: DXA analysis showing types of dislocations present. Green denotes Shockley partials 1/6<112>, purple stair-rod dislocations 1/6<110>, dark blue perfect dislocations ½<110>, yellow Hirth dislocations 1/3<001>, and light blue Frank partials 1/3<111>.

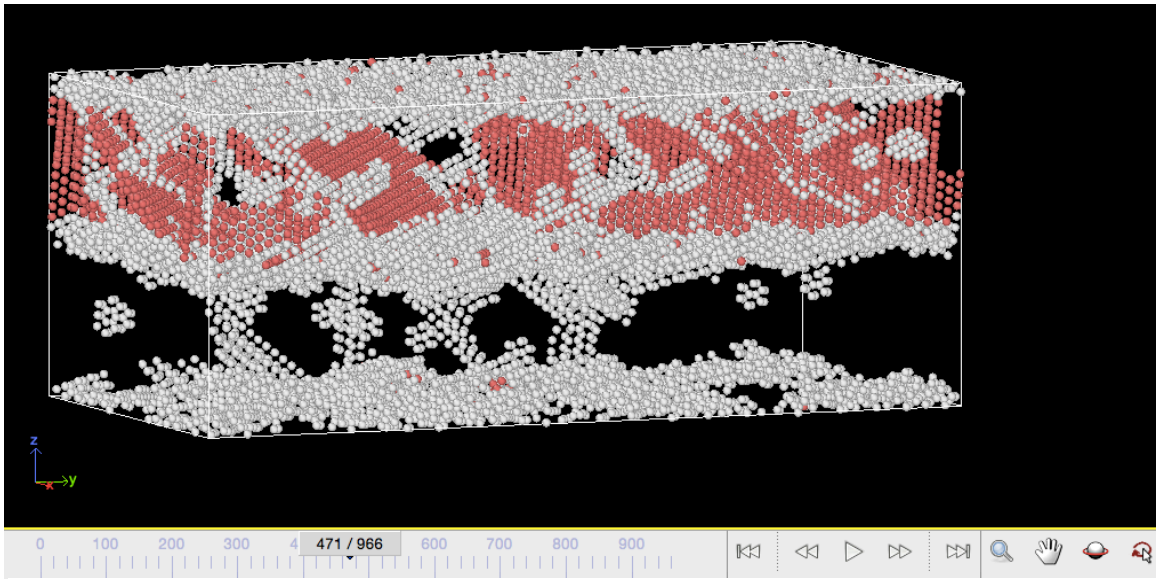

Figure 13 – Dislocation structure at 47.1% strain. Network of stacking faults in Cu layer shown in red. Stacking faults observed to participate in transmitting dislocations through interface.

3.1.3. Choosing Which Rotations to Keep

Atoms can get caught in the cores of dislocations, leading to large stretches and widely varying rotations between subsequent compression steps. For this reason, we only consider the rotations of perfect atoms in the Cu and Nb layers that are not caught in dislocations. Considering the rotation of perfect atoms can yield the "true" rotation of the lattice spatially. The rotation algorithm described in section 2 generates rotation matrices and stretch matrices. Large stretches can be identified and used to smooth over rotation matrices of atoms that get caught in dislocation cores. Consider the following pseudo-code:

```
1 for each stretch matrix calculate a norm
3 for each atom i
4         for every step j of simulation
5                 if norm(stretch(i,j)) is outside of [range]
6                         R(i,j) = I    %smooth rotation to identity matrix
7                 end
8         end
9 end
```

The code generates a cell of smoothed rotation matrices, which can then be accumulated into a total rotation by left multiplying rotation matrices. For compression step j:

$$R_{j,tot} = \prod_{k=0}^{k=j-1} R_{j-k} \quad (12)$$

$R_{j,tot}$ is then be converted to an axis angle pair.

Stretches within a certain range are considered as a way to filter out the perfect atoms from those caught in dislocation cores. An ideal stretch matrix $S_{applied}$ is the strain state applied to the simulation box of the material. As an example, take

$$S_{applied} = \begin{pmatrix} 1 & 0 & 0 \\ 0 & 1.001 & 0 \\ 0 & 0 & 0.999 \end{pmatrix} \quad (13)$$

This corresponds to 0.1% rolling tension along the y-direction and 0.1% compression in the z-direction per step. Now define

$$norm = Norm(diag(S_{ij}) - diag(S_{applied})) \quad (14)$$

Where Norm is the Euclidean norm and S_{ij} is the actual stretch between nearest neighbor triads on subsequent compression steps. For the PVD model, the distribution of stretch norms in the Cu layer is shown for 1000 atoms at 6% compression before plastic deformation, and at 6.1% compression after the onset of plastic deformation.

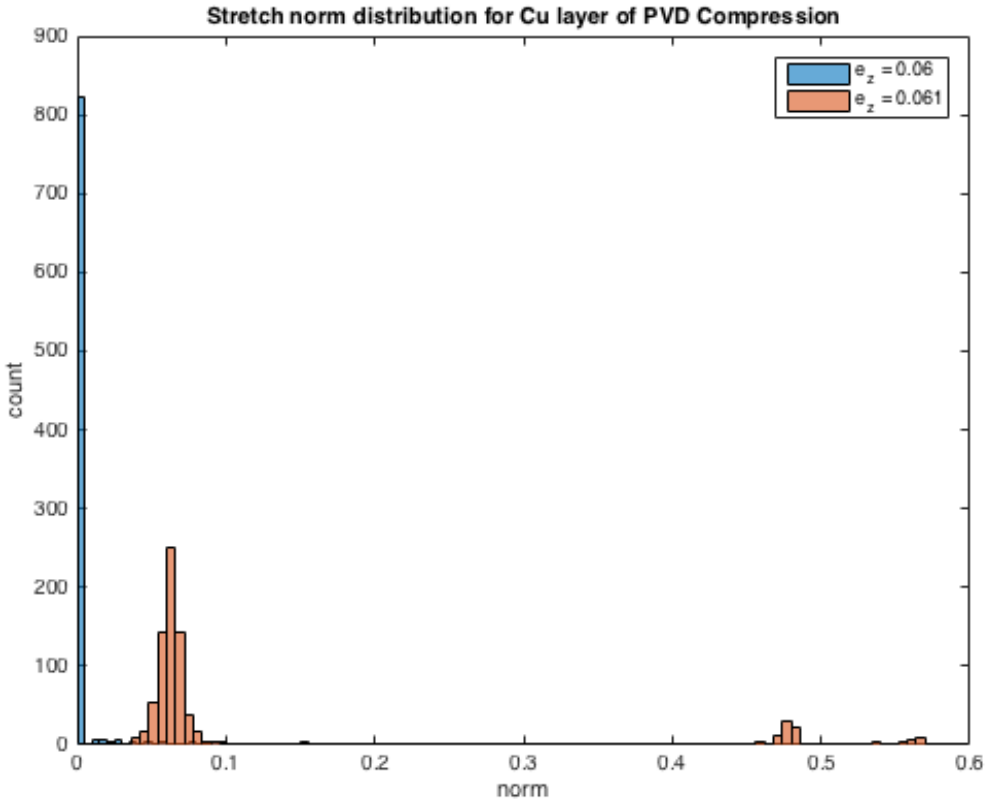

Figure 14 – Distribution of stretch norms before and after onset of plastic deformation at 6 and 6.1% strain. Plastic field of dislocation that passes through Cu alters stretch distribution from elastic background.

The stretch norm distribution before the onset of plastic distribution is concentrated at 0, implying that the lattice is deformed elastically according to the applied stretch state. After the onset of plastic deformation, the stretch norm distribution splits into three regions. The majority of stretch norms are clustered around a peak centered at $norm \simeq 0.7$, and the rest of the norms are centered around two smaller peaks

at higher values. It is assumed that the smaller peaks at higher stretch norms correspond to atoms caught in dislocation cores, which are highly strained, localized regions of the lattice. Dislocations exert a stress field on the lattice as a whole, explaining the deviation of all stretch norms from the peak in the elastic regime. Mean stretch norms are plotted along with standard deviations in Figure 15.

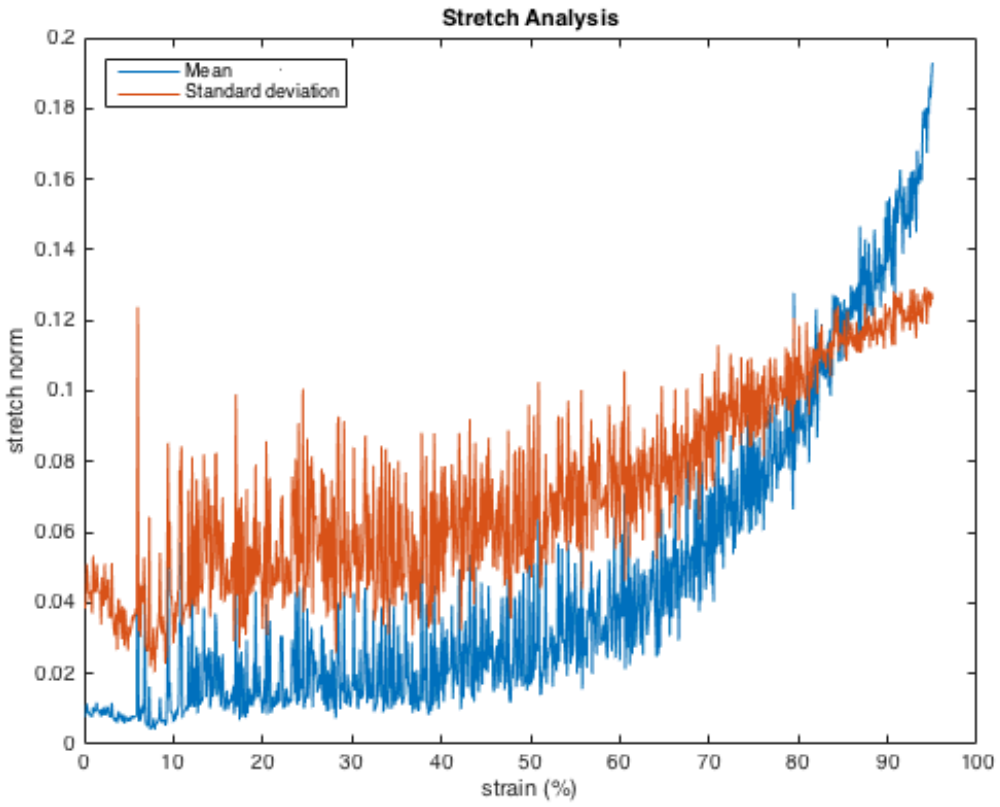

Figure 15 – Mean stretch norms over the course of the simulation, plotted along with standard deviations. Spikes in mean norm correspond to a change in stretch distribution, which in turn corresponds to a change in rotation.

Rotations are only accumulated (not smoothed over) for atoms with stretch norms smaller than the average stretch norm on a given compression step. This assumption is found to preserve rotation events observed in Ovito at the onset of plastic deformation.

3.1.4. Rotation Plots for Compression of the PVD Model

The rotation accumulation plot for 1000 Cu atoms is shown in Figure 16 (Top) along with some typical trajectories for individual atoms (Bottom). Some cross sections of the rotation accumulation plot are shown in Figure 17 at 10%, 30%, and 90% strain. The mean cumulative rotation angle for 1000 Cu and 1000 Nb atoms are plotted in Figure 18.

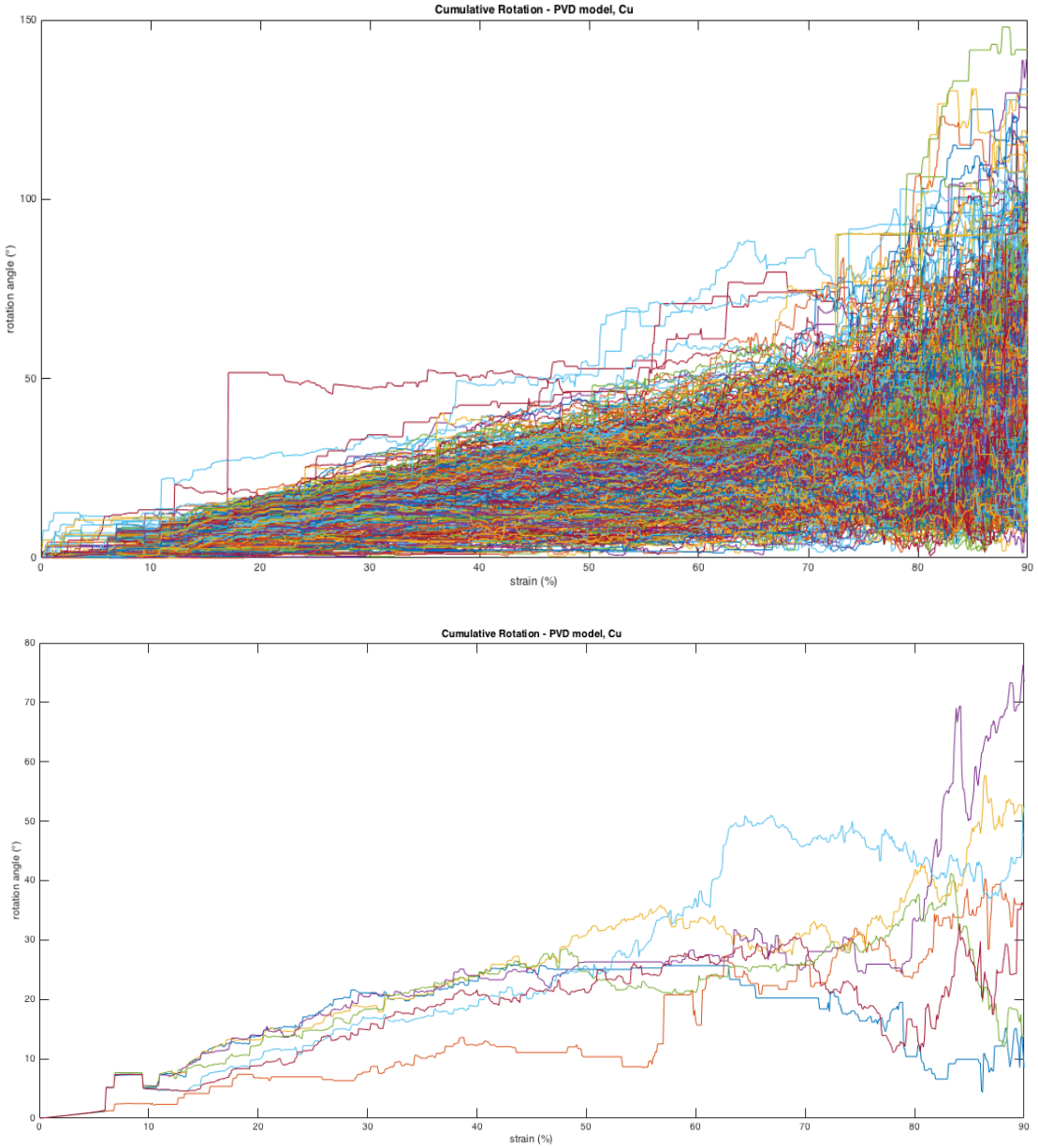

Fig 16 – Rotation accumulation plot for 1000 Cu atoms in PVD model (top) along with some typical trajectories (bottom).

The individual rotation trajectories rise and fall in densely packed bundles, with bundles splitting off from each other at certain strains. The splitting process averages out over strain and a unimodal distribution of rotations develops at strains > 20% from an initially multi-peaked rotation distribution at strains < 20%. In Figure 16, the orange rotation plot splits from the others at the onset of plastic deformation. Two possible reasons are as follows:

1. Some rotation matrices are smoothed over corresponding to atoms caught in dislocation cores, leading to a split in the rotation plot after discrete rotation events.
2. The rotations vary spatially across the lattice after the passage of dislocations through the lattice.

Observations using marker atoms in Ovito visually suggest that rotations across the Cu lattice are uniform at the onset of plastic deformation, implying that option 1 is the case: some rotations are smoothed over by the stretch filter, leading to splits in the rotation bundle plot. Histogram cross sections of the cumulative rotation plot in Figure 17 further verify the origins of the splitting process.

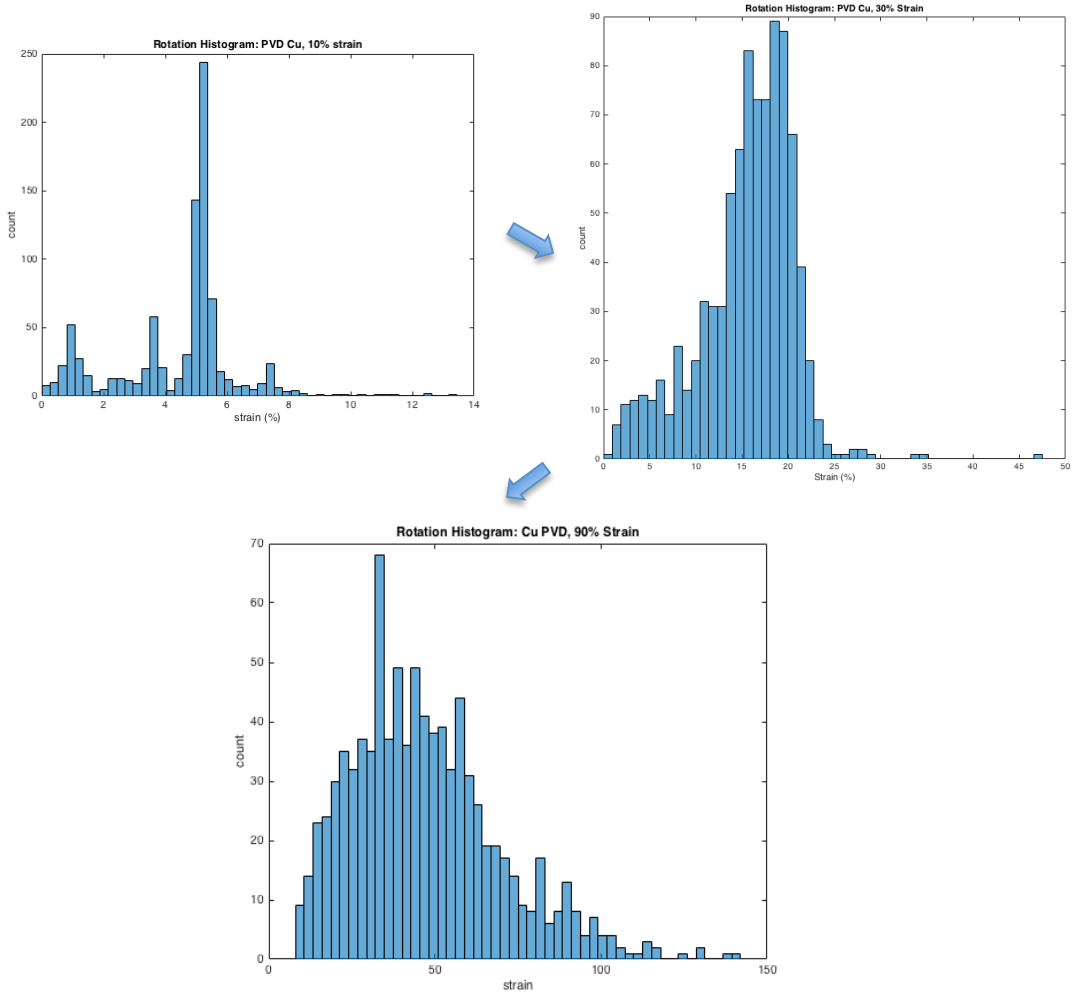

Fig 17 – Rotation histograms for Cu atoms in PVD model at 10%,30%, and 90% strain

At 10% strain, four rotation peaks arise due to the accumulated effects of smoothing events as dislocation pass through the material. At 30% strain, more dislocations have passed through the Cu, leading to even more smoothing of rotations and splits in the rotation plot. As the number of cumulative smoothing events becomes large past 20% strain, the distribution of rotations appears unimodal.

Such smoothing to a single peaked distribution can mask the true rotations of the material. The distribution of rotations at 30% strain is skewed left and the distribution at 90% strain is skewed right. Left skewness at 30% could come from some atoms getting repeatedly caught in dislocation cores. With many rotations smoothed over, cumulative rotation is small for those atoms. The right skewness at 90% strain is more intriguing, and could be an indication of grain refinement in the Cu layer at high strains.

Grains are regions of a metal that are rotated differently, separated by a boundary across which rotation changes discontinuously. At high strains, it is plausible that dislocation structures could stabilize into grain boundaries, leading to a multi-grained, or poly-crystalline, structure. The right skewness at 90% strain suggests a bimodal rotation distribution with one small peak centered around 90° rotations and a much larger peak centered around 30°. By 90% strain, almost every atom has been caught in a dislocation core at some point. The rightmost peak could indicate a minority of atoms that have not been caught in many dislocation cores. A way to get more reliable data to track whether new grains have been formed would be to regenerate common neighbor lists throughout the simulation. This would reinitialize nearest neighbor atoms which may have moved far apart, and could have the desired effect of reducing the spread in the rotation distribution to more precisely track rotation at large strains > 20%.

Average rotation plots for 1000 Cu and Nb atoms are shown in Figure 18. The plot picks out the initial rotations in both materials, with the rotation of Nb occurring later than the rotation of Cu at a smaller angle, as observed in Ovito. At 50% strain, rotation in the Cu layer is 23°+/-8° and rotation in the Nb layer is 17°+/-6°, where the uncertainty is given by one standard deviation away from the mean on either side. As discussed earlier, the uncertainty is inherent to the smoothing process and could also come from spatial variation in rotation, including grain refinement at high strains. At strains greater than 70%, mean cumulative rotation angles and standard deviations increase faster than the lower strain regime. Such a sharp increase in mean and standard deviation could be evidence for grain refinement, whereby the rotation distribution becomes bimodal and standard deviation from the mean increases.

For the PVD model rolled in the transverse direction, mean rotation at 50% strain was 17°+/-4° for Cu and 20°+/-6° for Nb. The mean rotations for Cu and Nb are within a standard deviation of each other in both simulations, and the data is not accurate enough to say that either Cu or Nb rotates more during the simulation. Both model rotate by similar amounts.

Unit rotation axes distributions are shown for PVD models rolled in the KS-direction in the Appendix, figure A1. The top figure shows the unit rotation axes distribution for Cu atoms at 50% strain on the surface of a unit sphere. The bottom left figure shows the projection of points on the sphere onto the x-y plane using a stereographic projection. The stereographic projection draws lines from the point (0,0,1) corresponding to the north pole of the sphere through all the axis points plotted on the sphere. The intersection of these lines with the xy-plane is known as a stereographic projection. The stereographic projection of unit rotation axes for Nb is shown in the bottom right-hand side of Fig. 1. Both projections for Cu and Nb show a clustering of points in certain regions of the unit plane, implying that within each layer, the axes are unimodally distributed about a single axis. These observations fit with the observation of the singly peaked rotation distributions at 50% strain. The clusters of axes points are

centered at different locations in the Cu and Nb layers, implying that different slip planes are operative in the layers during deformation, as expected.

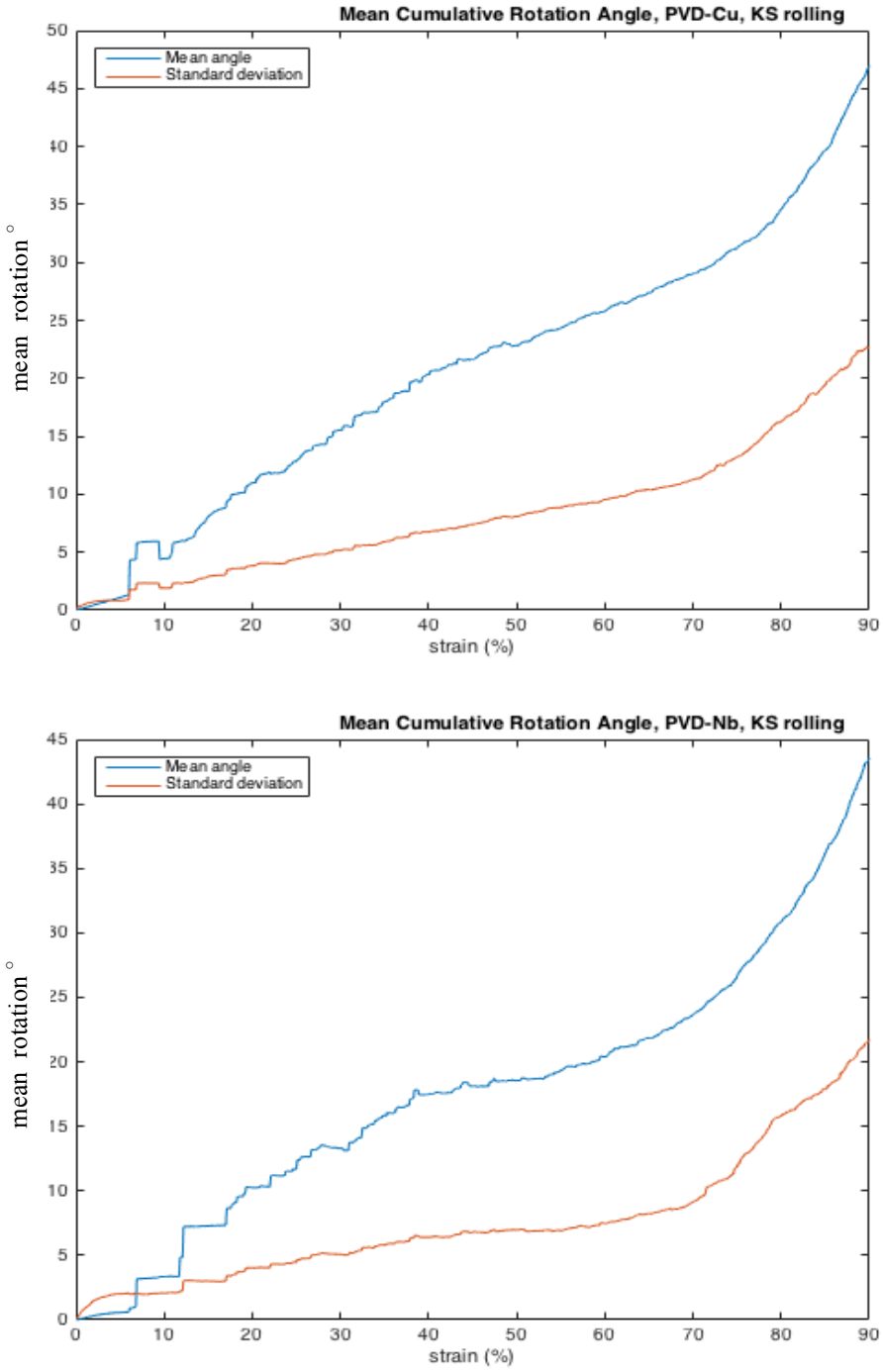

Figure 18 – Mean rotation of Cu and Nb layers in PVD model along with standard deviations. This model has rolling along the KS orientation, corresponding to the typically observed texture.

3.2. ARB Model

Stress-strain curves for the ARB model rolled in the <110>Cu || <111> Nb rolling direction and the transverse, faceted direction are shown in the Appendix Figure A2. Similar to the PVD stress-strain curves, the ARB models reach a steady-state at high strains past 70%. We denote the first model the ARB-KS model and the second the ARB-TD model, even though the TD interface also exhibits a KS orientation.

At the onset of plastic deformation, Shockley partials at the interface produce stacking faults for both rolling models, shown for the ARB-KS model in Figure 19.

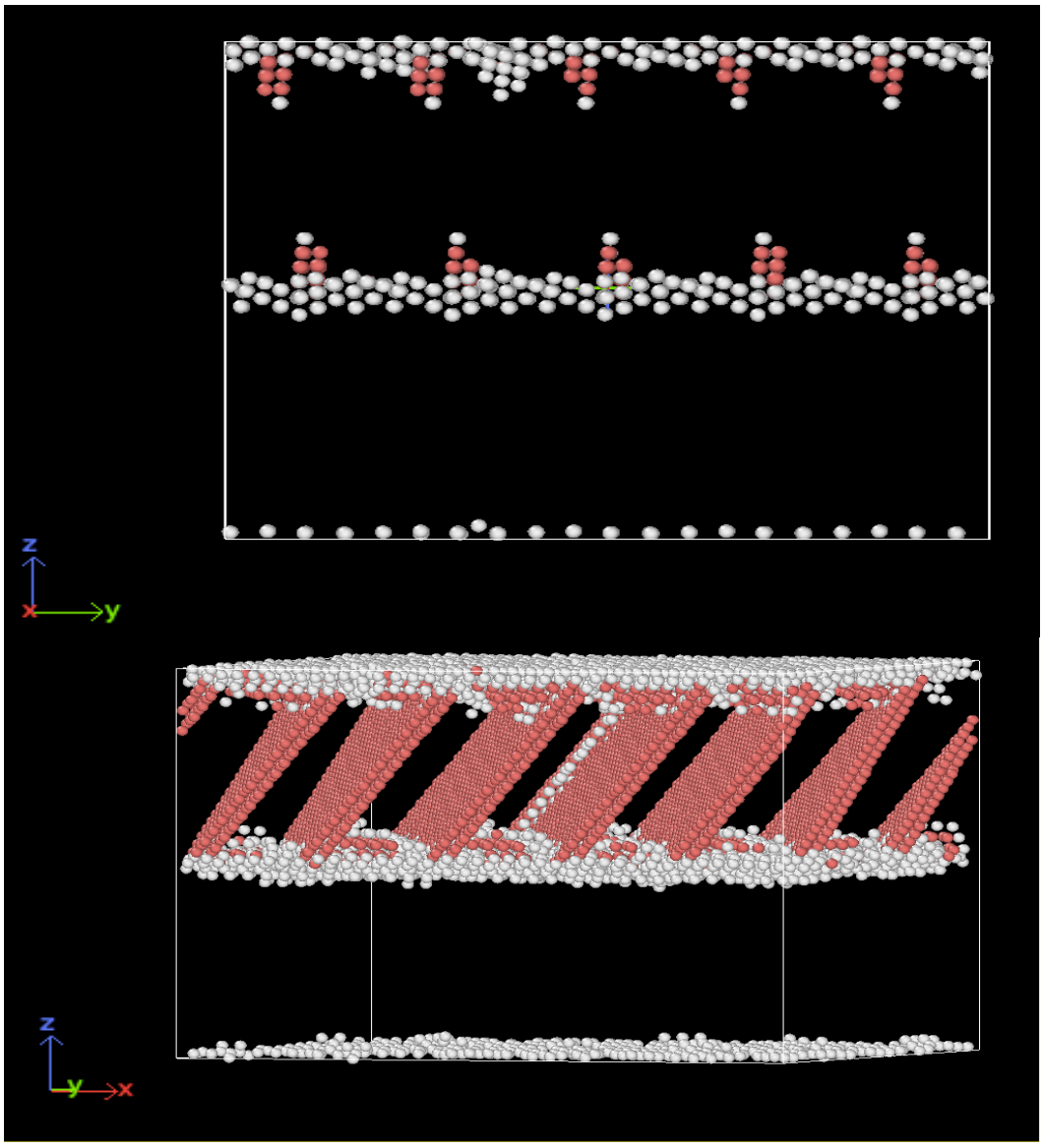

Figure 19 – ARB-KS model before and after onset of plastic deformation at 5.2% strain. Shockley partials at interface lead to the formation of stacking faults

Twinning is observed in the ARB-TD model throughout plastic deformation, unlike the ARB-KS or PVD models. Twinning is a separate form of plastic deformation from slip that can operate simultaneously. Unlike slip, deformation twins suddenly reorient a layer of the lattice to create a coherent boundary between the original layer orientation and deformed orientation [4]. Deformation twins in Cu are associated with glide of Shockley partials on adjacent planes [35]. The formation of a twin in the simulation is shown at the bottom of Figure 20 along with a zoomed out image of the entire Cu lattice. A single stacking fault is depicted on the bottom left with a slip step of 1/6<112> between red HCP layers. During twinning, a second stacking fault shifts the green layer of perfect atoms on top of the first stacking fault by 1/6<112>, leading to two coherent mirror images that constitute a stable twin. Twins are observed to persist for longer periods of strain than stacking faults. Twinning during ARB deformation may have a role in the stability of the experimentally observed interface character.

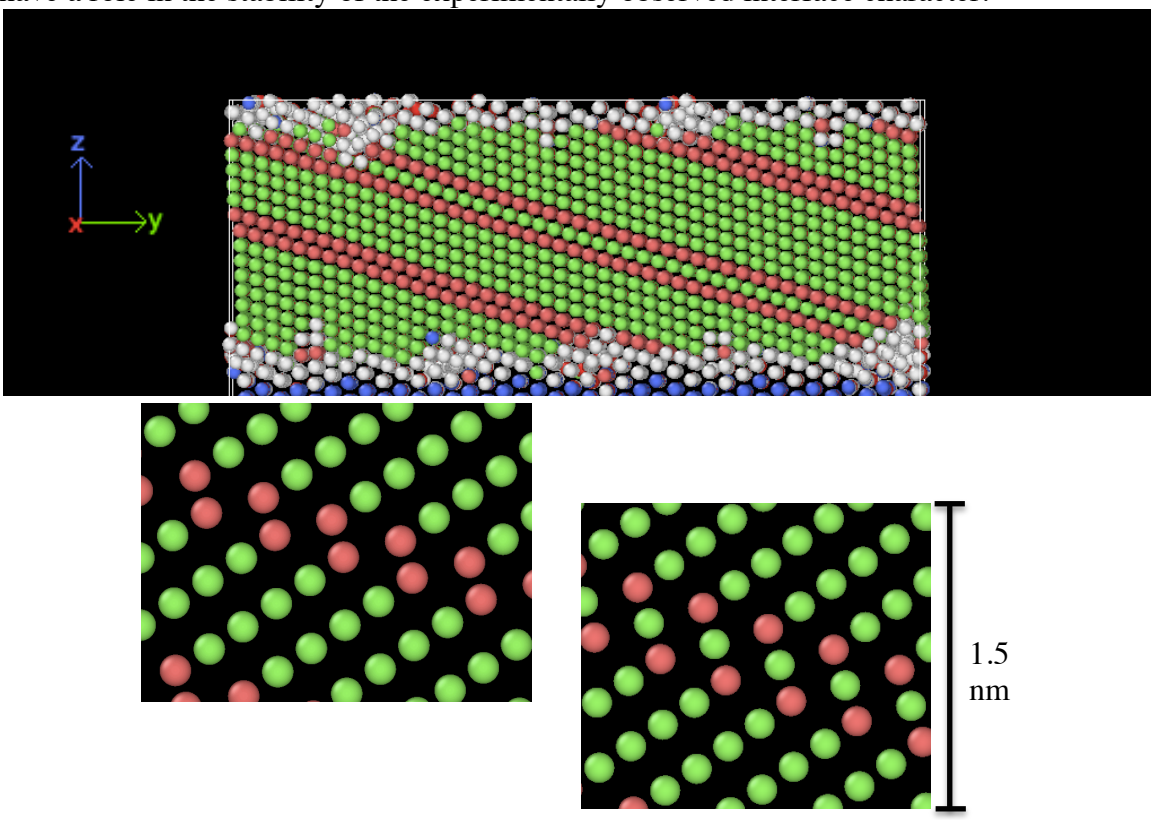

Fig 20 – ARB-TD model at 6.7% strain, showing a twin boundary. Illustration of twin formation

Figures A2 and A3 in the Appendix show the mean rotation of Cu and Nb in both ARB models. For rolling along the KS direction, mean rotation at 50% strain was 17°+/-8° for Cu and 17°+/-7° for Nb. For rolling along the TD direction, mean rotation at 50% strain was 25°+/-14° for Cu and 8°+/-5° for Nb. Initial pressures in the TD simulation were higher than initial pressures in the KS simulation, which could explain the high relative standard deviations in the TD simulation. Some atoms started with high initial rotations due to pressure changes on the first compression step, leading to a wider spread in rotation values for the entire simulation. As discussed in 2.2, initial pressures are

sensitive to initial simulation box size. Since standard deviations are high, any steady states that are reached could be masked by noise in the simulation caused by stretch filtering.

3.3. PVD Seed Model

The PVD Seed Model was compressed in increments of 1% in the z-direction and volume conserving tension was applied in the y-direction along the <110> Cu ||<111>Nb direction. The stress strain curve below shows that the polycrystalline model has a lower yield strength than the bicrystal models. Lower yield strength is expected because of the defective grain boundaries, which act as nucleation sites for dislocations under compression. The yield strength of the composite is around 1 GPa, within the characteristic range of yield strengths of nano-crystalline materials and Cu-Nb nano-composites [36]. Past 20% strain, the stress strain curve shows oscillations about a stress value of ~0.7 MPa.

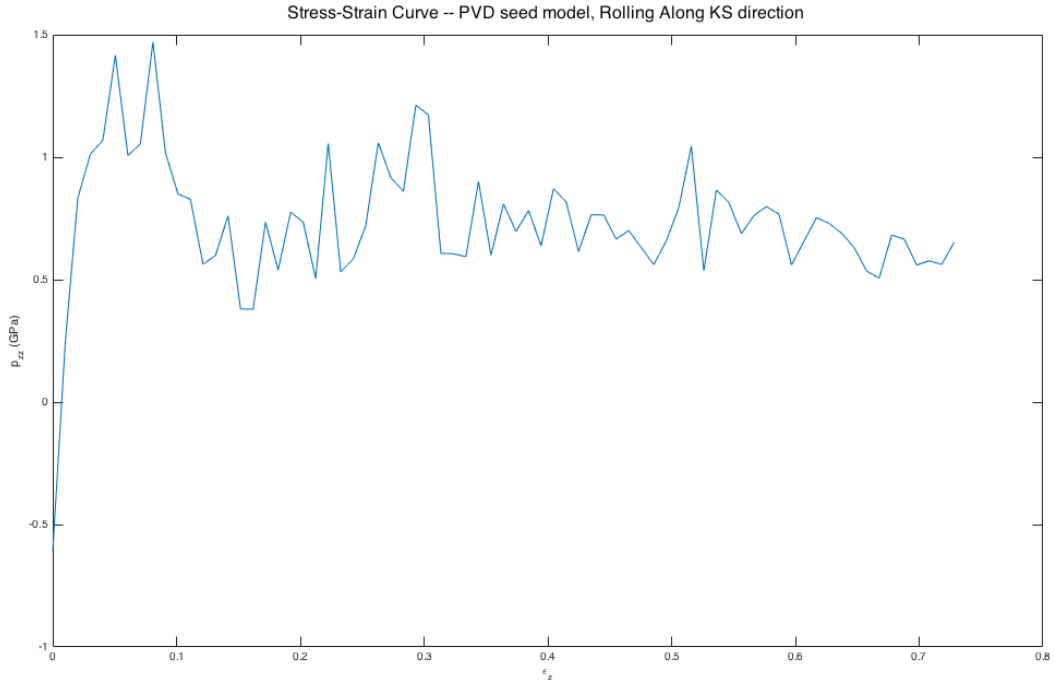

Figure 21 – Stress strain curve for final PVD-seed model rolled along KS direction

Figure 22 shows the model at 13% strain. Red marker atoms highlight initially horizontal cross sections through the PVD Cu and Nb layers and also mark a grain in the nano-crystalline copper structure. On the right of Fig 22, the dislocation structure of the Cu layer is shown. Stacking faults are observed to nucleate from the interface and cut through the PVD-Cu layer. Tangles of dislocations are present at grain boundaries between grains. As compression progresses, stacking faults within the nanocrystalline Cu grains cut into the PVD-Cu layer. At 60-70% strain, the Cu and Nb layers consolidate to the thickness of a single grain, and at 80% strain the Nb layers pinch off from a wavy interface, shown in Figure 23. At 80% strain, the layer thicknesses are about 4 nm each. At layer thicknesses as small as 4 nm, pinching off can be expected, and is not an

absolute indication that the PVD seed interface is not stable. Because of the immiscibility of Cu and Nb, there is little intermixing between layers, even at very large strains.

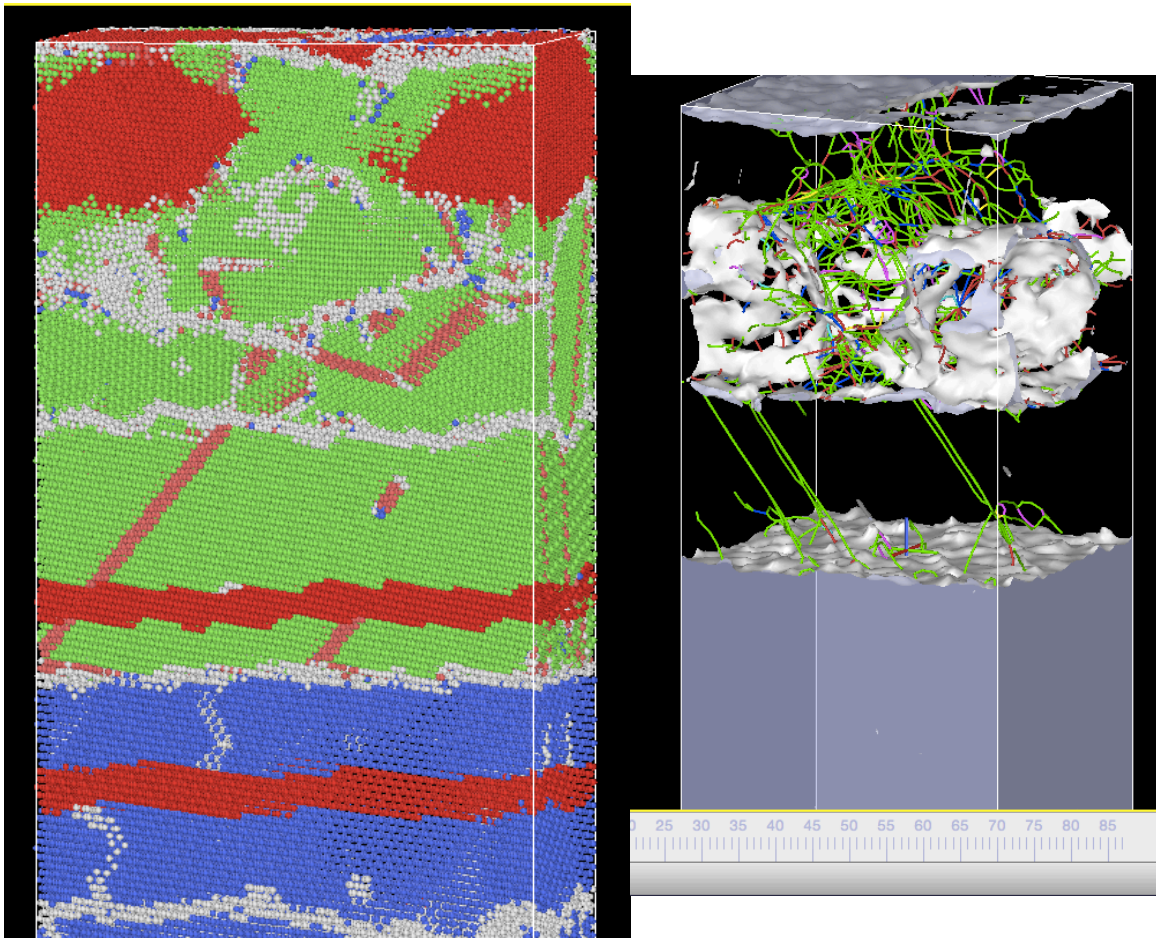

Figure 22 – PVD seed model at 13% strain with rotation markers on left and dislocation structure on right

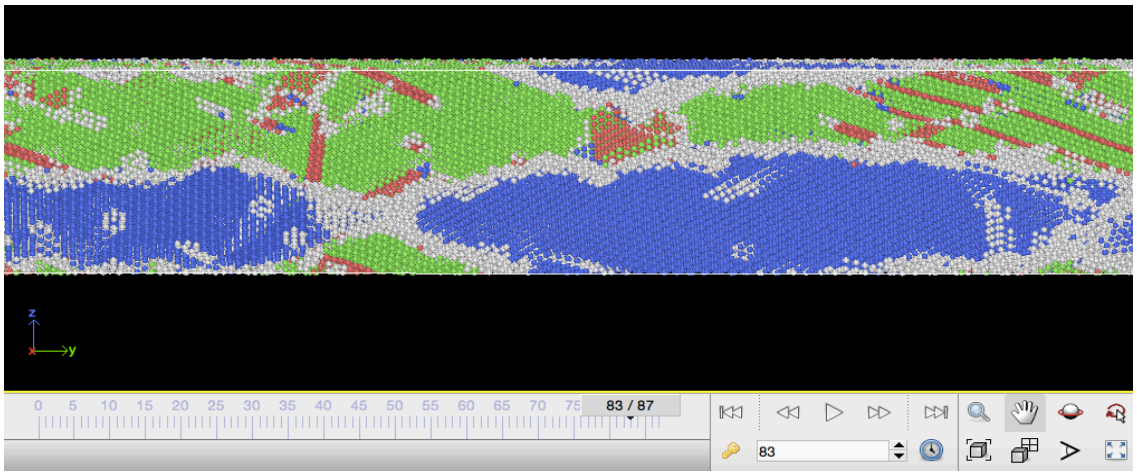

Figure 23– PVD seed model at 83% strain, Nb layers pinching off.

Rotations were analyzed for 10,000 atoms each in the PVD-Cu and PVD-Nb layers. The results in Figure 25 show average rotations at 50% strain of 21°+/-7° for Cu and 18°+/-7° for Nb. A histogram of rotations at 80% strain is given in Fig. 24 along with the rotation axes distribtuion. Both distributions are unimodal, indicating that a single grain is rotating under compression. Note that atoms from the nano-crystalline grains were not considered in the rotation analysis, nor were rotations about the interface between polycrystalline Cu and Nb. Rotation in the polycrystalline model appears similar to rotation in the standalone PVD model. Whether this is a result of the actual materials physics or uncertainty in the rotation analysis is discussed in the next section.

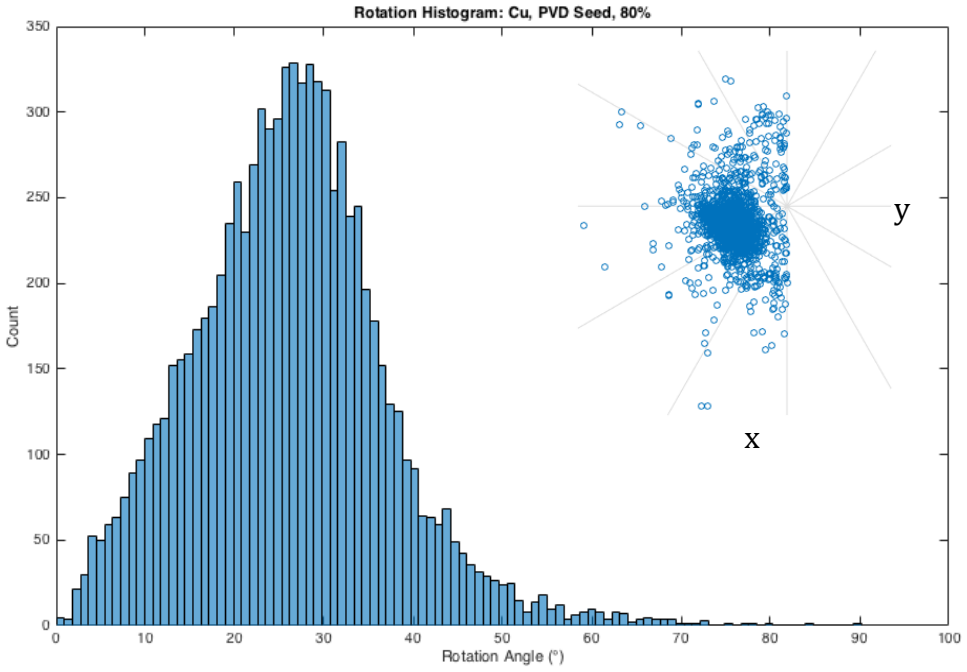

Figure 24 – Rotation histogram at 80% strain for Cu layer of PVD seed model along with unit rotation axes distribution.

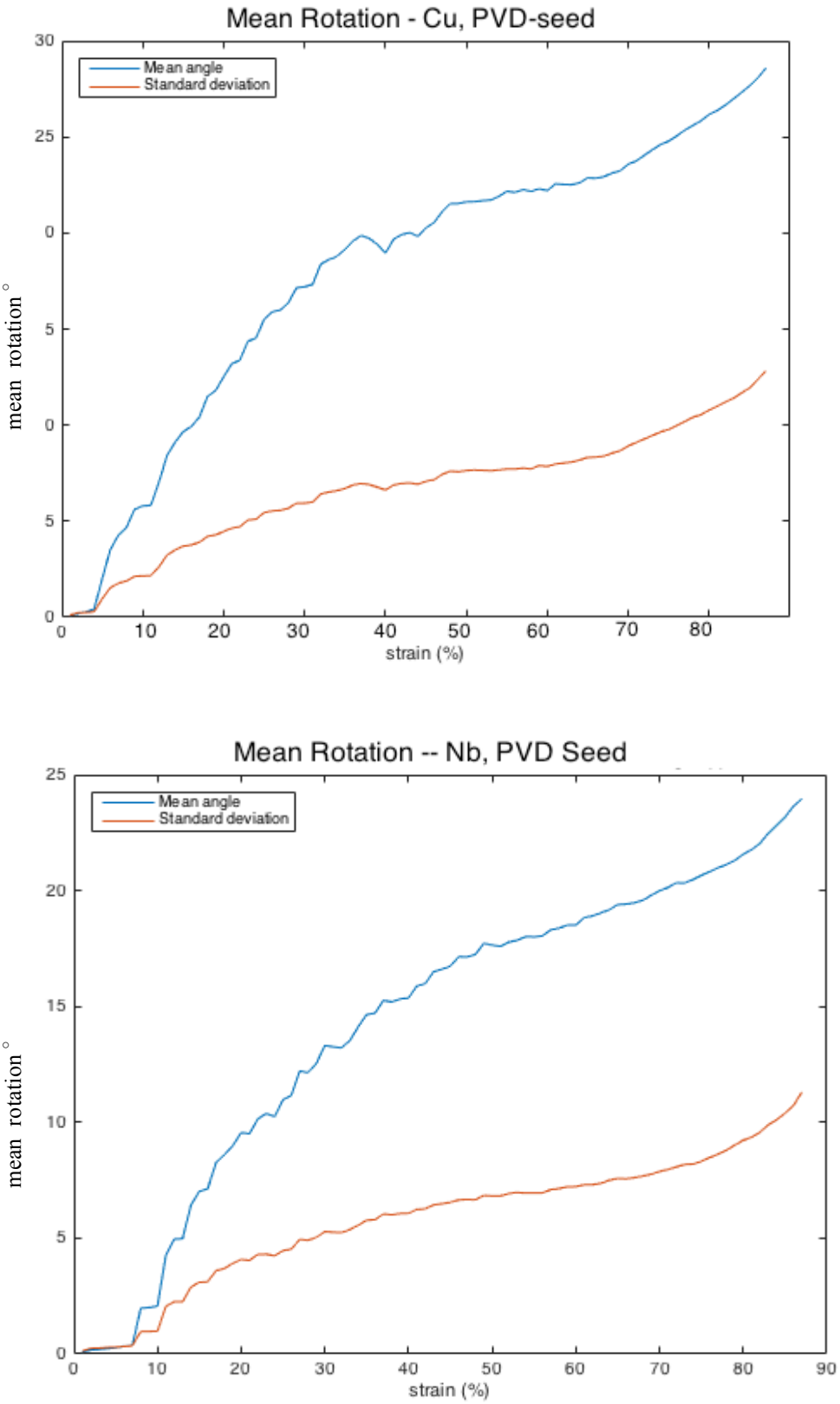

Figure 25 – Mean rotation of Cu and Nb layers in PVD-seed KS model.

3.4. Summary of Results and Future Directions

The rolling results for all of the models analyzed are summarized in the table below for 50% strain:

Model:	PVD, KS	PVD, TD	ARB, KS	ARB, TD	PVD Seed, KS
θ_{Cu}	23°+/-8°	17°+/-4°	17°+/-8°	25°+/-14°	21°+/-7°
θ_{Nb}	17°+/-6°	20°+/-6°	17°+/-7°	8°+/-5°	18°+/-7°

The rotations are all of comparable size and cannot be differentiated due to the high standard deviation of the analysis. It is apparent, however, that the Cu and Nb layers *do* rotate. This finding is significant because it contradicts the experimentally observed plastic stability of compressed PVD and ARB composites, implying that some factors are contributing to plastic stability in real experiments that are *not* present in the simulation. Such factors could include thermally activated dislocation mechanisms, multiple grain interactions, or constraints imposed by free surfaces. Each of those factors not present in the simulation offers an interesting direction for future work, discussed in the conclusion.

Neither the Cu nor Nb layer appears to consistently rotate more than the other, with the exception of Nb in the ARB-TD model, which rotates the least of any model. The rotation axes distributions for the Cu layers of the three models rolled in the KS direction at 50% strain are similar. The axes cluster around three different 30° increments in the polar rθ plane. The evenly spaced offsets between the rotation axes clusters of different models can be interpreted as different {111} slip planes that activate during plastic deformation within Cu. The axes distributions for rotation of Nb layers in all models are also uni-modal, with different mean axes observed than Cu rotations. Crystals have been found to rotate in the direction of slip under compression. Which slip planes activate depends on the interface structure of the model being compressed, the component crystals, and the chaotic nature of molecular dynamics simulations. Running the same simulation twice could lead to initial slip along different {111} type planes. The observation that crystals under compression often rotate into the direction of slip is important, and provides a first order justification for why the KS interface occurs frequently in highly strained FCC-BCC composites.

Two Crystal Plasticity Finite Element (CPFE) studies have been published about rolled Cu-Nb interfaces. *Beyerlein et al*. found that at 75% strain, ARB interfaces only rotated 5° in Cu about <110> and 3° in Nb about <110>. In contrast, PVD interfaces were found to be unstable at 75% strain, with rotations of 27° in Cu about <110> and 30° in Nb about <111> [37]. *D. Raabe et al*. found that for initial layer thicknesses of four microns in PVD composites, Cu layers rotated up to 20° and Nb layers up to 10° at 50% strain [22]. For initial layer thicknesses of 75 nm, very little rotation was observed in the CPFE model for either Cu or Nb at 50% strain, with Cu rotating up to 5° and Nb 3°. Both simulations took into account thermally induced dislocation motion. Though molecular statics operates at zero temperature, it generates more geometric information than CPFE techniques, specifically regarding dislocation activity in Cu and Nb. The only results in the present simulation that match those above concern the instability of the stand-alone PVD interface under compression. At 75% the model has rotations of around 30° in both Cu and Nb, similar to the findings of *Beyerlein et al*.

The PVD seed model appears to be unstable under compression, like the standalone PVD interface. The ARB model also appears to be plastically unstable, but this result contradicts both experiments and other simulations, and could therefore imply that temperature effects play a significant role in plastic stability. The disagreement further merits a re-surveying of the techniques used in this analysis with an eye for improvement. Listed below are seven ways to improve the compression simulation and rotation analysis in the future:

1. Re-initialize nearest neighbor lists after a certain number of strain steps. Smoothing rotation via a stretch filter leads to rotation trajectories splitting even when rotation is spatially homogeneous. Re-initializing nearest neighbor lists would re-initialize the splitting process, leading to more accurate results with lower standard deviation.
2. Consider all of the atoms in each model. Only 1000 Cu atoms and 1000 Nb atoms were considered in the PVD and ARB models, and only 10000 atoms in each layer were considered in the PVD seed model. Full statistics on the models will give more accurate results for rotations and axes distributions.
3. Visualize rotations spatially. Such visualization would help analyze further whether the rotation analysis is properly dealing with dislocation cores and could give insight into where rotations are taking place in the lattice and when grain refinement is taking place, if ever.
4. Consider a simpler rotation framework that only tracks one nearest neighbor vector for each atom. In addition to intuitively matching the rotation of layers with marker atoms in Ovito, the framework could lead to straightforward generation of rolling textures for Cu and Nb at different strains.
5. Track the rotation of the grains in the PVD seed model in addition to the PVD layers. Rotations of the grains could shed light on stabilizing or destabilizing effects from the grain structure on the seeded interface.
6. Further optimize the initial interface spacings in the PVD seed model and ARB-TD model to eliminate any pressure effects on rotation results.
7. Analyze several different seed layers. Data has already been generated for the CD interface (see section 2.1.4), and could further inform the plastic stability / instability of seeded Cu-Nb interface models.

4. Conclusion

The PVD interface appears to be unstable at high compressive strains in both the stand-alone PVD model and the seeded PVD model. Instability is shown by significant rotation of Cu and Nb layers from their initial orientations for large strains > 20%. The standard deviations of rotation results are large, and further refinement of the rotation analysis could lead to more accurate results and a revised conclusion for high strains. The rotation analysis has been shown to successfully track rotations that occur at the onset of plastic deformation. The disagreement between this simulation and experimentally observed plastic stability of rolled PVD and ARB nano-composites indicates that the geometric and energetic factors present in the simulation do not tell the whole story of plastic stability. Variables not considered like temperature dependent dislocation mechanisms, grain interactions, or finite material effects (with free surface boundary

conditions) could play a significant role in plastic stability. ARB could be simulated at finite temperatures by adding an annealing step after each compression step using MD techniques, or equivalently by varying the strain rate of compression.

Many nano-composites with desirable properties are still limited to the lab-scale and cannot be made in bulk quantities. Accumulative roll bonding offers a strategy to scale up these limited nano-materials to industrially feasible sizes using the seed layer technique. Though a proof of concept for the seed layer technique has yet to be shown, ARB has already been used to successfully produce one bulk nano-material, and can likely be leveraged to produce more. Molecular dynamics and statics approaches offer a powerful way to analyze and visualize the deformation of a lattice under roll bonding constraints at an atomistic level. Paired with plasticity simulations at larger length scales and hands on experiments, atomistic simulation techniques are poised to explore the fundamental principles coupling deformation and interface evolution. Understanding the relationship between strain pathways and interface evolution will allow the design of a new class of bulk nano-materials that could make nuclear power more efficient and sustainable and space exploration more resilient to extreme environments.

5. Appendix

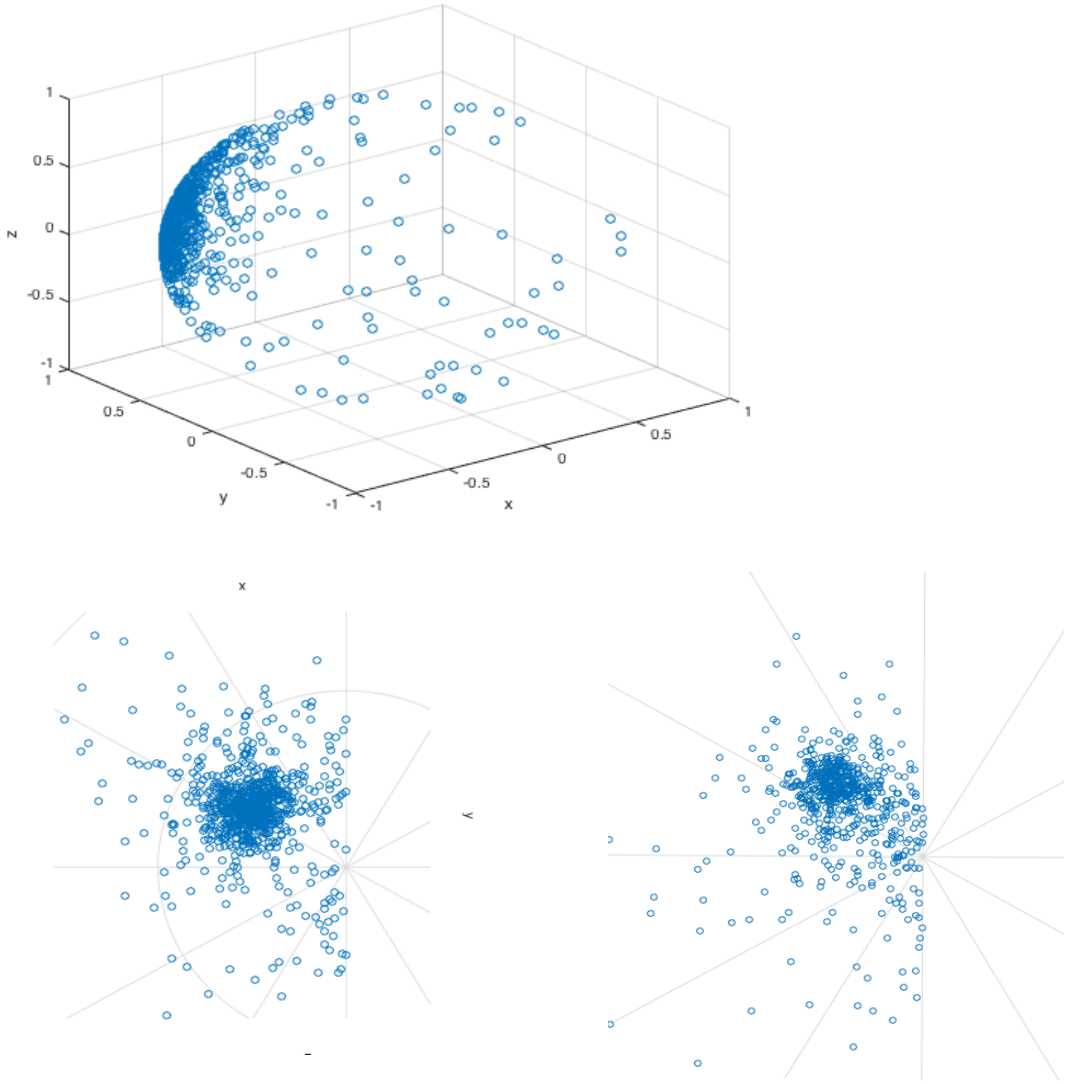

Figure A1 – Stereographic projections of unit rotation axes distributions for Cu and Nb at 50% strain. Both show a single clustering, implying one dominant rotation axis. Clustering is offset between Cu and Nb by 15 degrees.

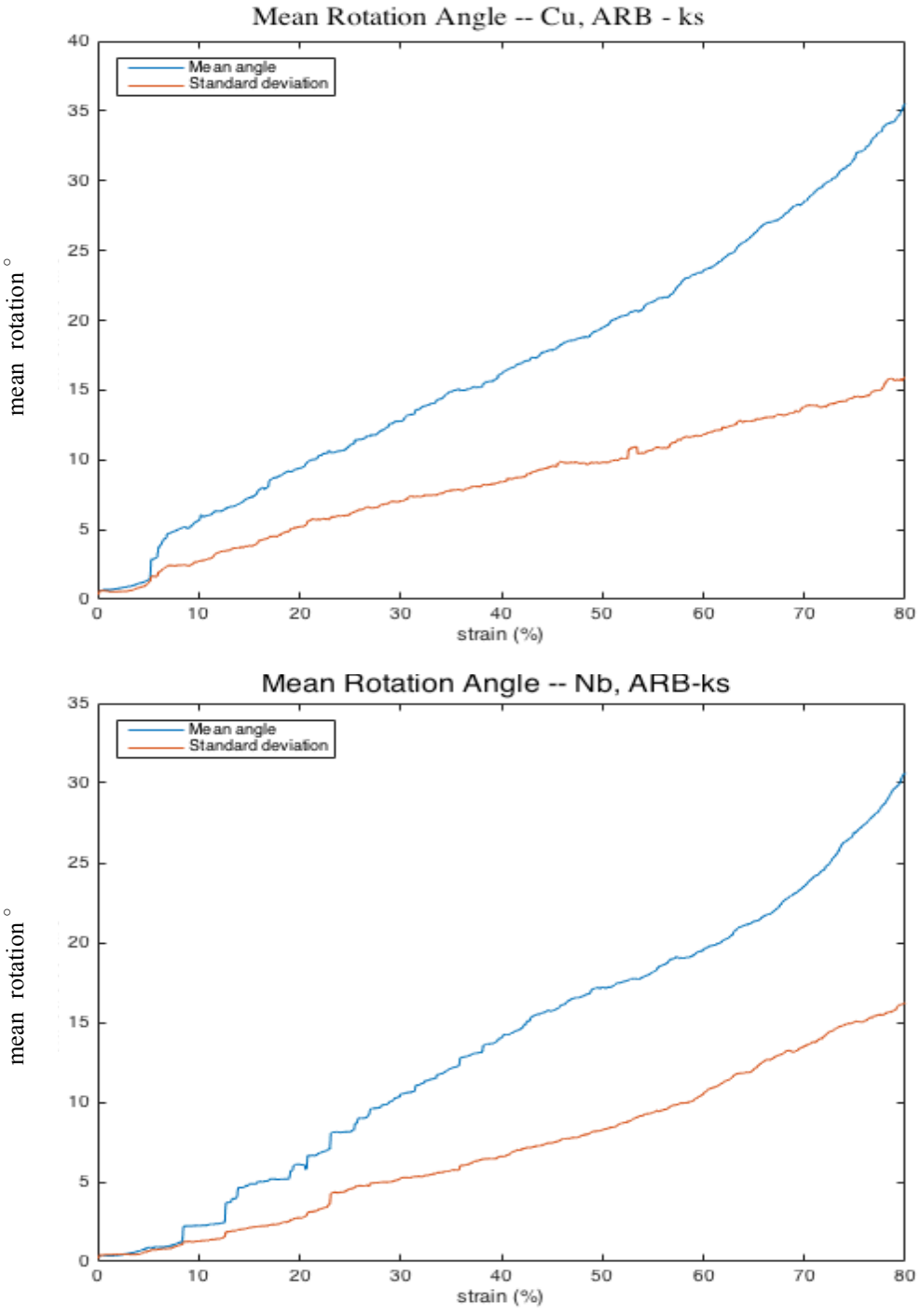

Figure A2 – Mean rotation of Cu and Nb layers in ARB-ks model along with standard deviations.

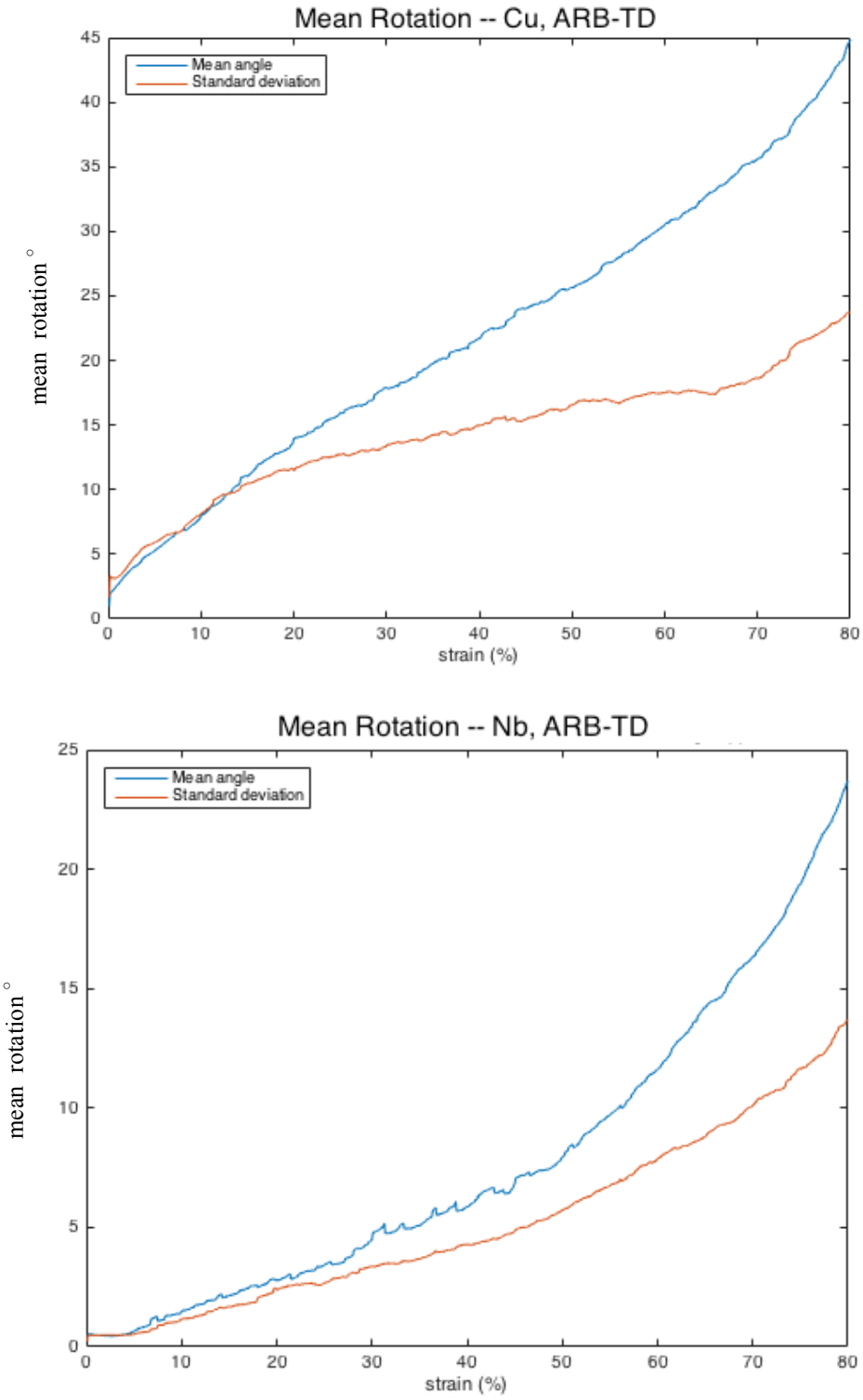

Fig A3– Mean rotation of Cu and Nb layers in ARB-TD model along with standard deviations.

6. References

[1] Zinkle, Steven J., and G. S. Was. “Materials challenges in nuclear energy.” Acta Materialia 61.3 (2013): 735-758.

[2] Han, W., Demkowicz, … Misra, A. (2013). “Design of Radiation Tolerant Materials Via Interface Engineering.” Advanced Materials, 25(48), 6975–6979.

[3] Mara, N. a., & Beyerlein, I. J. (2015). Interface-dominant multilayers fabricated by severe plastic deformation: Stability under extreme conditions. Current Opinion in Solid State and Materials Science, 19(5), 1–12

[4] Beyerlein, I. J., Demkowicz, M. J., Misra, a., & Uberuaga, B. P. (2015). Defect-interface interactions. Progress in Materials Science, 74(October), 125–210.

[5] BES Workshop report Basic Research Needs for Advanced Nuclear Energy Systems (2006), www.science.doe.gov/bes/reports/files/ANES_rpt.pdf.

[6] Misra, a., Demkowicz, M. J., Zhang, X., & Hoagland, R. G. (2007). The radiation damage tolerance of ultra-high strength nanolayered composites. Jom, 59(9), 62–65. doi:10.1007/s11837-007-0120-6

[7] Ewing, R. C. (2015). Long-term storage of spent nuclear fuel. Nature Materials, 14(3), 252–257. doi:10.1038/nmat4226

[8] https://en.wikipedia.org/wiki/Fukushima_Daiichi_nuclear_disaster

[9] Lee, S. B., Ledonne, J. E., Lim, S. C. V, Beyerlein, I. J., & Rollett, a. D. (2012). The heterophase interface character distribution of physical vapor-deposited and accumulative roll-bonded Cu-Nb multilayer composites. Acta Materialia, 60(4), 1747–1761. doi:10.1016/j.actamat.2011.12.007

[10] Snel, Jeremy. Competing deformation mechanisms in ARB Cu/Nb metallic multilayers as a function of layer thickness and temperature. IMDEA Materials Institute (2016)

[11] Mara, N. a., & Beyerlein, I. J. (2014). Review: Effect of bimetal interface structure on the mechanical behavior of Cu-Nb fcc-bcc nanolayered composites. Journal of Materials Science, 49(19), 6497–6516. doi:10.1007/s10853-014-8342-9

[12] Beyerlein IJ, Mayeur JR, Zheng S, Mara NA, Wang J, Misra A. Emergence of stable interfaces under extreme plastic deformation. Proceedings of the National Academy of Sciences of the United States of America. 2014;111(12):4386-4390. doi:10.1073/pnas.1319436111.

[13] Beyerlein, I. J., Mayeur, J. R., Zheng, S., Mara, N. a, Wang, J., & Misra, A. (2014). Emergence of stable interfaces under extreme plastic deformation. Proceedings of the National Academy of Sciences, 111(12), 4386–4390. doi:10.1073/pnas.1319436111

[14] Demkowicz, M. J., & Thilly, L. (2011). Structure, shear resistance and interaction with point defects of interfaces in Cu-Nb nanocomposites synthesized by severe plastic deformation. Acta Materialia, 59(20), 7744–7756. doi:10.1016/j.actamat.2011.09.004

[15] A. Stukowski. Visualization and analysis of atomistic simulation data with OVITO - the Open Visualization Tool. Modelling Simul. Mater. Sci. Eng. 18 (2010), 015012. http://www.ovito.org/index.php

[16] Stukowski, A. (2012). Structure identification methods for atomistic simulations of crystalline materials. Model. Simul. Mater. Sci. Eng., 20, 45021. doi:10.1088/0965-0393/20/4/045021
[17] G. Gottstein, D.A. Molodov, L.S. Shvindlerman. Interface Sci, 6 (1998), pp. 7–22
[18] Fan, Zhigang, et al. "Simulation of polycrystalline structure with Voronoi diagram in Laguerre geometry based on random closed packing of spheres." Computational materials science 29.3 (2004): 301-308.
[19] Demkowicz, M. J., & Hoagland, R. G. (2008). Structure of Kurdjumov-Sachs interfaces in simulations of a copper-niobium bilayer. Journal of Nuclear Materials, 372(1), 45–52. doi:10.1016/j.jnucmat.2007.02.001
[20] Wang, J., Kang, K., Zhang, R. F., Zheng, S. J., Beyerlein, I. J., & Mara, N. a. (2012). Structure and property of interfaces in ARB Cu/Nb laminated composites. Jom, 64(10), 1208–1217. doi:10.1007/s11837-012-0429-7
[21] Misra, a., Hirth, J. P., Hoagland, R. G., Embury, J. D., & Kung, H. (2004). Dislocation mechanisms and symmetric slip in rolled nano-scale metallic multilayers. Acta Materialia, 52(8), 2387–2394. doi:10.1016/j.actamat.2004.01.029
[22] Jia, N., Raabe, D., & Zhao, X. (2016). Crystal plasticity modeling of size effects in rolled multilayered Cu-Nb composites. Acta Materialia, 111, 116–128. doi:10.1016/j.actamat.2016.03.055
[23] Plimpton, Steve, Paul Crozier, and Aidan Thompson. "LAMMPS-large-scale atomic/molecular massively parallel simulator." Sandia National Laboratories 18 (2007).
[24] Mishin, Yu, M. Asta, and Ju Li. "Atomistic modeling of interfaces and their impact on microstructure and properties." Acta Materialia 58.4 (2010): 1117-1151.
[25] https://en.wikipedia.org/wiki/Conjugate_gradient_method
[26] Vinogradov, O. G. (2010). On reliability of molecular statics simulations of plasticity in crystals. Computational Materials Science, 50(2), 771–775. doi:10.1016/j.commatsci.2010.10.009
[27] https://en.wikipedia.org/wiki/K-d_tree
[28] Allen, Mike P., and Dominic J. Tildesley. Computer simulation of liquids. Oxford university press, 1989.
[29] https://en.wikipedia.org/wiki/Periodic_boundary_conditions
[30] Demkowicz, M. Kinematics of Plasticity Due to Lecture Glide. 3.22 Lecture Notes, Lecture 12
[31] Nizolek, T., Beyerlein, I. J., Mara, N. a., Avallone, J. T., & Pollock, T. M. (2016). Tensile behavior and flow stress anisotropy of accumulative roll bonded Cu-Nb nanolaminates. Applied Physics Letters, 108(5), 051903. doi:10.1063/1.4941043
[32] Misra, a., Hirth, J. P., Hoagland, R. G., Embury, J. D., & Kung, H. (2004). Dislocation mechanisms and symmetric slip in rolled nano-scale metallic multilayers. Acta Materialia, 52(8), 2387–2394. doi:10.1016/j.actamat.2004.01.029
[33] Martínez, E., Uberuaga, B. P., & Beyerlein, I. J. (2016). Interaction of small mobile stacking fault tetrahedra with free surfaces, dislocations, and interfaces in Cu and Cu-Nb. Physical Review B, 93(5), 054105. doi:10.1103/PhysRevB.93.054105
[34] A. Stukowski and K. Albe. Modelling Simul. Mater. Sci. Eng. 18, 085001 (2010)

[35] Zhu, Y. T., Liao, X. Z., & Wu, X. L. (2012). Deformation twinning in nanocrystalline materials. Progress in Materials Science, 57(1), 1–62. doi:10.1016/j.pmatsci.2011.05.001
[36] Schiøtz, Jakob, and Karsten W. Jacobsen. "A maximum in the strength of nanocrystalline copper." Science 301.5638 (2003): 1357-1359.
[37] Mayeur, J. R., Beyerlein, I. J., Bronkhorst, C. a., Mourad, H. M., & Hansen, B. L. (2013). A crystal plasticity study of heterophase interface character stability of Cu/Nb bicrystals. International Journal of Plasticity, 48, 72–91. doi:10.1016/j.ijplas.2013.02.006
[38] Lattice Planes and Miller Indices, DoITPoMS (2008): http://www.doitpoms.ac.uk/tlplib/miller_indices/index.php
[39] *https://en.wikipedia.org/wiki/Slip_(materials_science)*